

ERASMUS MUNDUS MSc PROGRAMME

COASTAL AND MARINE ENGINEERING AND MANAGEMENT

CoMEM

STUDY OF FATIGUE DESIGN
ON MARINE CURRENT TURBINE SUPPORT STRUCTURE
BALI - INDONESIA

UNIVERSITY OF SOUTHAMPTON

June 2011

Tubagus Ary Tresna Dirgantara

324496669

The Erasmus Mundus MSc Coastal and Marine Engineering and Management is an integrated programme organized by five European partner institutions, coordinated by Delft University of Technology (TU Delft). The joint study programme of 120 ECTS credits (two years full-time) has been obtained at three of the five CoMEM partner institutions:

- Norges Teknisk- Naturvitenskapelige Universitet (NTNU) Trondheim, Norway
- Technische Universiteit (TU) Delft, The Netherlands
- City University London, Great Britain
- Universitat Politècnica de Catalunya (UPC), Barcelona, Spain
- University of Southampton, Southampton, Great Britain

The first year consists of the first and second semesters of 30 ECTS each, spent at NTNU, Trondheim and Delft University of Technology respectively.

The second year allows for specialization in three subjects and during the third semester courses are taken with a focus on advanced topics in the selected area of specialization:

- Engineering
- Management
- Environment

In the fourth and final semester an MSc project and thesis have to be completed.

The two year CoMEM programme leads to three officially recognized MSc diploma certificates. These will be issued by the three universities which have been attended by the student. The transcripts issued with the MSc Diploma Certificate of each university include grades/marks for each subject. A complete overview of subjects and ECTS credits is included in the Diploma Supplement, as received from the CoMEM coordinating university, Delft University of Technology (TU Delft).

Information regarding the CoMEM programme can be obtained from the programme coordinator and director

Prof. Dr. Ir. Marcel J.F. Stive
Delft University of Technology
Faculty of Civil Engineering and geosciences
P.O. Box 5048
2600 GA Delft
The Netherlands

SUMMARY

Clean Green energy is being desired all over the globe. It gives cleaner world and healthier environment to live. Most of the green energy resources such as tidal and wave are freely available in large amount and also sustainable. On the other hand, the energy demand is increasing along with population growth. Therefore, researchers are developing the technology of energy converter from these resources to support human activities, business and leisure. Indonesia an archipelago country with plenty of narrow strait and surrounded by two oceans makes this tidal energy extraction looks promising.

A pioneer study in Bali Strait as the reference site is selected among other prospective sites. Bali strait has relatively shallow water depth, high current density and high energy demand to support Bali Island and its tourism board. As the equipment of tidal energy converter is placed in severe condition for relatively long period, hence it has to be strength resistance and fatigue resistance. Fatigue failure will cause integrity failure which mostly occurs in the joint connections and at the base of support structure. Therefore, Fatigue design plays an important role in the development of tidal energy converter. Fatigue analysis on MCT support structure is based on experience and engineering judgement. Two established industries, oil and gas exploration and offshore wind turbine, are tailored into marine current turbine development. In addition, a range of representative cases is selected in this dissertation.

To conclude, the fatigue service life for MCT support structure located in Bali strait has fulfil the minimum required of 80 years (20 years service life with factor of safety 4.0) with various alternatives. Contrary to the offshore wind turbine (OWT) with natural period at soft-soft range, the recommended natural period range for MCT is placed at soft-stiff range. This because of the MCT support structure requires stiffer and more compact structure as they are exposed to more severe loading compare to OWT. However, another analysis should be conducted such as strength resistance and accidental limit stress in order to have a complete design. On the other hand, Environment Impact Assessment should be prepared as well. In addition, this study might be the first study of fatigue assessment in MCT support structure and should be considered as an opening to a further renewable energy development.

ACKNOWLEDGMENTS

Many people have contributed directly and indirectly in preparing this dissertation. Therefore, the author would like to thank them all very sincerely. Support and knowledge sharing are the biggest and the greatest driver to complete this dissertation.

The author would like to express his deepest gratitude to:

- Prof. Marcel Stive, for the chance in MSc CoMEM 2009/2011.
- Mariette van Tilburg and Madelon Burgmeijer, for all the good news and supporting us while doing MSc courses.
- Prof. A.S. Bahaj, for this big opportunity in renewable energy under your supervision at the University of Southampton.
- Luke Blunden, for daily supervision on the project.
- Prof. Nichols, Southampton CoMEM Coordinator.
- Prof. Øivind A. Arntsen, Trondheim CoMEM Coordinator.
- Indra Wirawan, Structure Head Department of PT Singgar Mulia.
- All my professors and lecturers in Southampton, Delft, and Trondheim.
- My parents and family for all their prayer and support.
- My wife Syndhi Purnama Sari and my baby boy Tubagus Muhammad Rasya Ibrahim Al-Arsy, my heart, my life, my home.
- All my CoMEM colleagues: Tam, Zeng, Ono, Lava, Xuexue, Ji, AP, Marli, Kevin, Adam, Cekar, Bruno, Fernanda, Cinthya, Mauricio, Ricardo and William.
- All my friends in Southampton, Delft, and Trondheim.

TABLE OF CONTENTS

SUMMARY

ACKNOWLEDGMENTS

TABLE OF CONTENTS.....	i
LIST OF FIGURES.....	iii
LIST OF TABLES.....	v
GLOSSARY OF TERMS.....	vi
LIST OF ABBREVIATIONS.....	vii
1 INTRODUCTION.....	1-1
1.1 Introduction.....	1-1
1.2 Problem Background.....	1-1
1.3 Aims and Objectives.....	1-2
1.4 Structure of the Report.....	1-2
1.5 Software Used.....	1-3
2 BASIC OF OFFSHORE, HYDRO AND TURBINE ENGINEERING.....	2-1
2.1 Introduction.....	2-1
2.2 General Terminology of MCT.....	2-1
2.3 Stochastic Process.....	2-2
2.4 Hydrodynamics.....	2-5
2.5 Turbine Description.....	2-14
2.6 Dynamics of Marine Current Turbine.....	2-19
2.7 Foundation.....	2-23
2.8 Limit State Design.....	2-24
3 FATIGUE DESIGN TERMINOLOGY.....	3-1
3.1 Introduction.....	3-1
3.2 Time Domain vs. Frequency Domain.....	3-1
3.3 Principles of Fatigue Analysis.....	3-2

3.4	Spectral Fatigue Analysis	3-4
3.5	Stress Concentration Factor.....	3-13
3.6	Fatigue Endurance	3-14
4	METHODOLOGY	4-1
4.1	Introduction	4-1
4.2	Overview of Methodology	4-1
4.3	Analysis Set-up Wave Induce Fatigue	4-2
4.4	Analysis Set-up Turbine Induce Fatigue.....	4-4
4.5	Description of the MCT Support Structure	4-5
4.6	Environment Data	4-5
4.7	Computer Model.....	4-8
5	ANALYSIS RESULT	5-1
5.1	Introduction	5-1
5.2	Mono-pile Structure.....	5-1
5.3	Gravity Base Structure	5-4
5.4	Tripod Structure.....	5-6
6	ECONOMICS AND OPTIMIZATION.....	6-1
6.1	Introduction	6-1
6.2	Financial Analysis	6-1
6.3	Support Structure Selection.....	6-2
6.4	Cathodic Protection	6-3
6.5	Weld Improvement.....	6-4
6.6	Inspection Strategy	6-4
7	CONCLUSION AND RECOMMENDATION	7-1
7.1	Conclusion.....	7-1
7.2	Recommendation.....	7-2

REFERENCES

APPENDICES

LIST OF FIGURES

Figure 2-1 : Overview of Marine Current Turbine Terminology 2-1

Figure 2-2 : Overview of Marine Current Turbine Support Structure 2-2

Figure 2-3 : Overview of Regular Wave 2-2

Figure 2-4 : Three Regular Wave Summed into One Irregular Wave 2-3

Figure 2-5 : Amplitude versus Frequency as Result from Fourier Transform..... 2-4

Figure 2-6 : JONSWAP and Pierson-Moskowitz Wave Spectra 2-6

Figure 2-7 : Actuator Disk Model 2-9

Figure 2-8 : Velocity and Static Pressure along the Stream Line 2-10

Figure 2-9 : Elements of a Blade 2-11

Figure 2-10 : Velocity and Load on Blade Element 2-12

Figure 2-11 : Lift and Drag Coefficient over Angle of Attack (Batten, 2006) 2-13

Figure 2-12 : Wind Turbine Power Curve (Shell, 2010)..... 2-15

Figure 2-13 : Power Coefficient versus Tip Speed Ratio (Batten, 2006) 2-16

Figure 2-14 : Power vs. Rotational Speed at Different Wind Velocities (Pijpaert, T., 2002). 2-17

Figure 2-15 : Power versus Wind Velocity V90-3.0MW (DUWIND) 2-17

Figure 2-16 : Stall and Pitch on a Hydrofoil..... 2-18

Figure 2-17 : Lift Coefficient versus Angle of Attack (Batten, 2006)..... 2-18

Figure 2-18 : 1-DOF mass-damper-spring system..... 2-20

Figure 2-19 : DAF versus Normalized Frequency 2-20

Figure 2-20 : Excitation Frequency of 1P and 3P Turbine [28] 2-21

Figure 2-21 : Occurrence of Wave Frequency with 1P and 3P Frequencies [38] 2-22

Figure 2-22 : Pile-Soil Interaction Foundation Model..... 2-23

Figure 3-1 : Harmonic Sinusoidal Wave and Harmonic Structure Response Wave 3-5

Figure 3-2 : Structure Transfer Function..... 3-6

Figure 3-3 : Selection of Frequencies for Detailed Analyses (API RP 2A)..... 3-8

Figure 3-4 : Overview Frequency Domain Spectral Fatigue Analysis [38] 3-13

Figure 3-5 : Typical S-N Curve for Structural Detail 3-15

Figure 4-1 : Overview of Fatigue Analysis Methodology for Current and Wave 4-2

Figure 4-2 : Water Depth Configuration for Monopile MCT Support Structure 4-5

Figure 4-3 : MCT Support Structure Configuration 4-5

Figure 4-4 : Tidal Constituents in Indonesia [22] 4-5

Figure 4-5 : Distribution of wave period for fatigue analysis at Pagerungan station [29] 4-7

Figure 4-6 : Distribution of wave period for fatigue analysis with 1p and 3P Plot 4-8

Figure 5-1 : Service Life of Monopile with Constant tw of 25mm at 40m Water Depth5-1

Figure 5-2 : Comparison Service Life Using Constant D and tw at 40m Water Depth5-2

Figure 5-3 : Comparison Service Life at Three Different Water Depth.....5-3

Figure 5-4 : Service Life of GBS at 40m Water Depth5-4

Figure 5-5 : Service Life of GBS at 30m Water Depth5-5

Figure 5-6 : Service Life of GBS at 20m Water Depth5-6

Figure 5-7 : Tripod structure 3D view and Top view.....5-6

Figure 5-8 : Service Life of Tripod at 40m Water Depth5-7

Figure 6-1 : IRR Sensitivity of Offshore Wind Farm (Shell, 2010)6-2

LIST OF TABLES

Table 2-1 : Fixity Depth of Different Types of Soil [4]	2-24
Table 3-1 : Time Series and Spectral Parameters for Waves	3-2
Table 4-1 : Spectral Fatigue Analysis Procedure	4-3
Table 4-2 : Current Data over Depth [29]	4-6
Table 4-3 : Percentage Wave Occurrence at Pagerungan station [29].....	4-7
Table 4-4 : MCT Natural Period Selection.....	4-8
Table 5-1 : Service Life of Monopile with Constant t_w of 25mm at 40m Water Depth.....	5-2
Table 5-2 : Service Life of Monopile with Constant D of 400mm at 40m Water Depth.....	5-3
Table 5-3 : Service Life of Monopile at 20m Water Depth	5-3
Table 5-4 : Service Life of Monopile at 30m Water Depth	5-4
Table 5-5 : Service Life of GBS at 40m Water Depth	5-5
Table 5-6 : Service Life of GBS at 30m Water Depth	5-5
Table 5-7 : Service Life of GBS at 20m Water Depth	5-6
Table 5-8 : Service Life of Tripod at 40m Water Depth	5-7

GLOSSARY OF TERMS

API X Prime	API S-N curve's without considering profile controlling between as-welded and adjoining base metal.
Bali Strait	Strait which separate Java Island with Bali Island, located in Indonesian archipelago.
Hot Spot Stress Transfer Functions	The hot spot stress amplitude per unit wave amplitude over a range of wave frequencies at each wave direction.
Hot Spot Stress	The range of maximum principal stress adjacent to the potential crack location with stress concentrations being taken into account.
Seastate	General condition of free surface on a large body of water (with respect to wind waves and swell) at a certain location and time. It characterized by statistics of wave height, period, and power spectrum.
Tidal Energy	Form of hydropower that converts the energy of tides into electricity or other useful forms of power.

LIST OF ABBREVIATIONS

ALS	Accidental Limit State
API	American Petroleum Institute
DNV	Det Norske Veritas
DOF	Degree of Freedom
FLS	Fatigue Limit State
IRR	Internal Rate of Return
LSD	Limit State Design
MCT	Marine Current Turbine
NPV	Net Present Value
OWT	Offshore Wind Turbine
RMS	Root Mean Square
SACS	Structure Analysis Computer System
SCF	Stress Concentration Factor
SLS	Service Limit State
TSR	Tip Speed Ratio
ULS	Ultimate Limit State
VIR	Value Investment Ratio

1 INTRODUCTION

1.1 Introduction

Clean Green energy is now being desired in all over the globe. It gives cleaner world and healthier environment to live with. Most of the green energy resources such as tidal and wave are freely available in large amount and also sustainable. On the other hand, the need of energy increases along with population growth. Therefore, scientists are developing the technology of energy converter from these resources to support human activities, business and leisure.

In the UK particularly, Marine Current Turbine (MCT) is now being developed in advance to support inland energy demand. The well known technology from oil and gas exploration and wind engineering are being the basic terminology in MCT development. Both technologies influence the design of MCT main components which are support structure and turbine.

As the MCT is exposed by severe and dynamic environment condition for a long-term period, strength resistance and fatigue resistance are indeed required. The dynamics of MCT makes it more liable to fatigue failure than strength failure. In specific, the endurance of MCT support structure due to fatigue failure will be the main consideration in this dissertation.

1.2 Problem Background

The marine current turbine support structure should be safe in the fatigue point of view and economically profitable. Precise information on environment condition and structure response is essential to gain both requirements.

Computer program is used to translate the environmental information into loadings on the support structure and the turbine. This enable engineers to model, simulate and analyse the dynamic behaviour of MCT efficiently and effectively. Even though no specialized software developed yet on MCT, approximation from offshore oil and gas based programs could be used with several parameters adjustment. Such programs however, need experienced users and extensive inputs.

On the design, loadings on support structure and turbine need to be combined since the approach techniques for both components are slightly different. The combination will be made in frequency domain with linear approximation. This method is more attractive compare to time series domain due to time effectiveness without losing the important parameters.

Indonesia an archipelago country with plenty of narrow strait and surrounded by two oceans makes this tidal energy extraction looks promising. A pioneer study in Bali Strait as the reference site is selected among other prospective sites. Bali strait has relatively shallow water depth, high current density and high energy demand to support Bali Island and its tourism board.

1.3 Aims and Objectives

The aim of this dissertation is to find the appropriate support structure for marine current turbine energy converter in a range of different environment conditions that is safe in fatigue design point of view and economically profitable.

The appropriate support structure could be achieved by milestones of objectives in the followings:

1. Finding a method to derive fatigue life of MCT support structure due to associate fatigue loadings.
2. Compare the support structures at design condition which give more advantage.
3. Produce a structured general guidance for fatigue design of MCT support structure.

1.4 Structure of the Report

This report is structured into four parts at seven chapters. It started with introduction to the thesis which contains the problem background, aims and objectives, structure of the report and the software used.

Chapter 2 provides the basic of offshore, hydro and turbine description. It covers the general terminology of the MCT, stochastic process of the environment condition, hydrodynamics, MCT description, the dynamics of MCT, foundation description and limit state design. Fatigue design terminology at the following chapter describes the principles of fatigue analysis, spectral fatigue analysis, stress concentration factors and fatigue endurance of the support structures. Both chapters are part of the literature review in the body of this thesis.

The general design methodology for MCT and computer modelling are illustrated in chapter 4. It adapted from fatigue design for an offshore jacket in the oil and gas industry.

Chapter 5 gives an overview of the analysis result for all support structure types. Overview on optimization of the support structure will be outlined in chapter 6 which consists financial analysis, support structure selection, cathodic protection, weld improvement and inspection

strategy. Chapter 7 summarizes the conclusions and gives a recommendation on the further development of marine current turbine design practice.

1.5 Software Used

The following computer programs were used in this thesis:

- SACS, offshore structural design package, Engineering Dynamic, Inc.
- EXCEL, spreadsheet program, Microsoft Inc.

2 BASIC OF OFFSHORE, HYDRO AND TURBINE ENGINEERING

2.1 Introduction

The basic of offshore, hydro and turbine engineering delivers parts of knowledge from each engineering subject to be tailored in one concept of Marine Current Turbine (MCT).

Section 2.2 describes the general MCT terminology. The basic stochastic process on wave is reviewed in section 2.3 followed by hydrodynamics description and calculation method in section 2.4. Section 2.5 gives an overview of the turbine and load calculation method. The dynamics of MCT and its foundation are out-lined in section 2.6 and 2.7 respectively. Finally, the limit state design is described in section 2.8.

2.2 General Terminology of MCT

The terminology for this thesis is shown in Figure 2-1 and Figure 2-2.

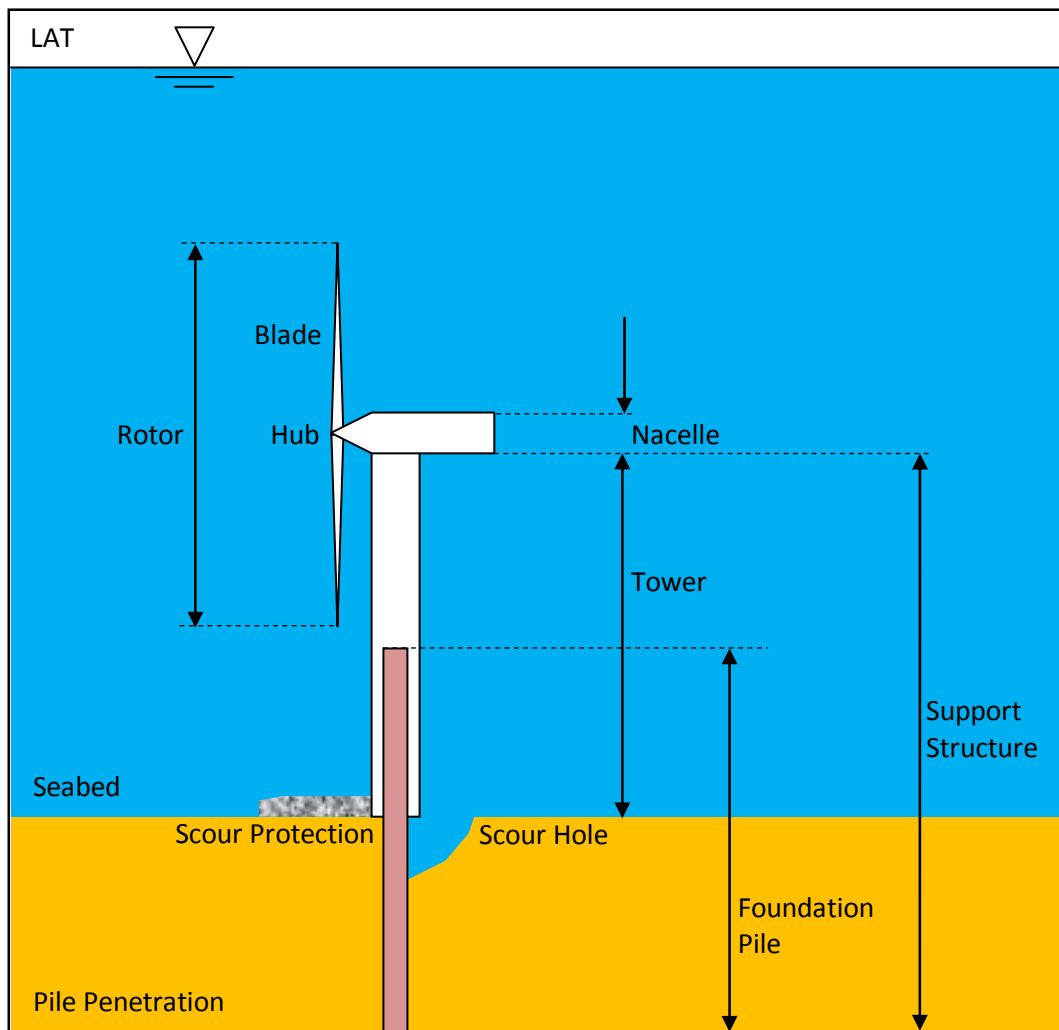


Figure 2-1 : Overview of Marine Current Turbine Terminology

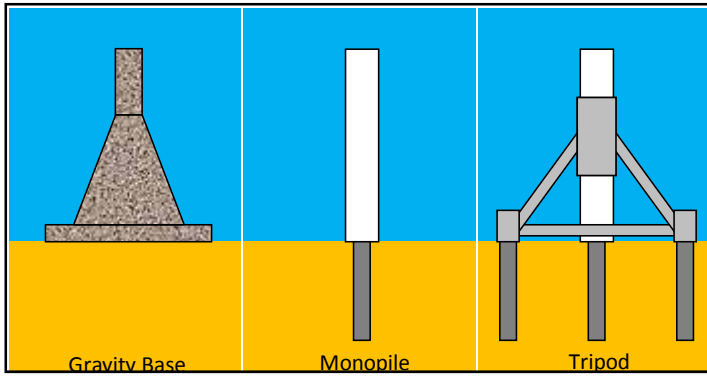


Figure 2-2 : Overview of Marine Current Turbine Support Structure

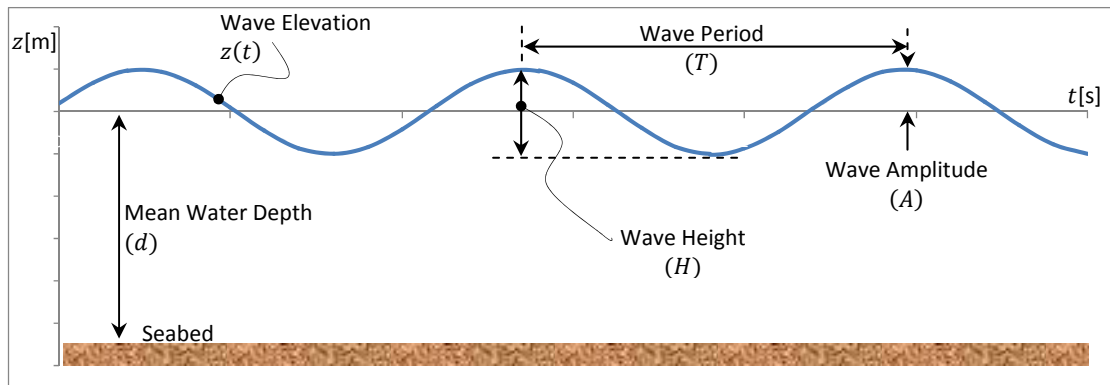


Figure 2-3 : Overview of Regular Wave

2.3 Stochastic Process

Stochastic or random process is a time-varying event that cannot be predicted or reproduced in detail. Environment loads are varies, stochastic in time and generally described as fluctuating time series loads. This type of data is hardly distinguished the characteristic of responses. Therefore, to make it more accessible, the time series data is translated into frequency domain through Fourier formulation. The result, spectrum of different characteristic responses can be seen easily.

2.3.1 Fourier Transform

Fourier transform is used to translate an event in time series into frequency domain. It assumed that a random signal can be represented by a sum of regular sinusoidal wave at specific amplitude, frequency and phase angle as shown in Figure 2-4. The single and sum of regular waves are represented by equation (2-1) and (2-2) respectively.

$$z(t) = A \sin (2\pi f \cdot t + \varphi) \tag{2-1}$$

$$\sum z(t) = \sum_{n=1}^N A_n \sin (2\pi f_n \cdot t + \varphi_n) \tag{2-2}$$

Where $z(t)$ = elevation of wave at time t [m]
 A = wave amplitude [m]
 f = wave frequency [Hz]
 φ = wave phase angle [rad]
 t = time [s]
 n = counter 1, 2, ..., N [-]

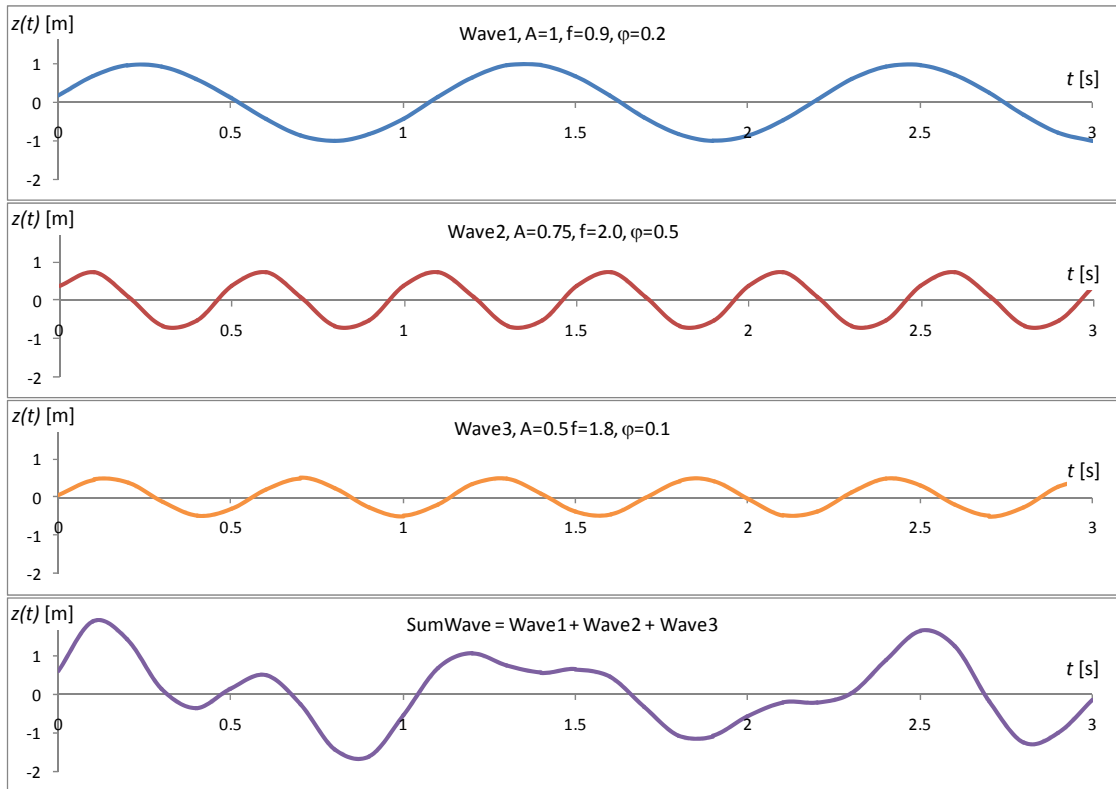


Figure 2-4 : Three Regular Wave Summed into One Irregular Wave

By reversing the sequence and assuming that the sum of wave or irregular wave is available, Fourier transform could be used to break it into several single regular waves as shown in equation (2-3) and (2-4).

$$z(t) = A_0 + \sum_{n=1}^N \{A_n \cos(2\pi f_n \cdot t) + B_n \sin(2\pi f_n \cdot t)\} \tag{2-3}$$

$$A_n = \frac{2}{T} \int_0^T z(t) \cos(2\pi f_n \cdot t) dt \quad \text{and} \quad B_n = \frac{2}{T} \int_0^T z(t) \sin(2\pi f_n \cdot t) dt \tag{2-4}$$

Where A_0 = mean amplitude of the wave ($A_0=0$ for sea wave) [m]
 A_n and B_n = Fourier coefficients [m]

f_n	= wave frequency of n^{th} Fourier component	[Hz]
T	= duration of measurement ($T = N \Delta t$)	[s]
Δt	= time step	[s]
n	= counter 1, 2, ..., N	[-]
N	= total number of time steps	[-]

Fourier transform of the wave amplitude as a function of frequency is shown in Figure 2-5 which is derived from the irregular wave in Figure 2-4. All the values are zero except at the frequencies of 0.9, 1.8 and 2.0 that have 1, 0.5 and 0.75 amplitude respectively. For phase angle, at the intermediate frequencies, a random scatter of angle applies while others are exactly the same as input value.

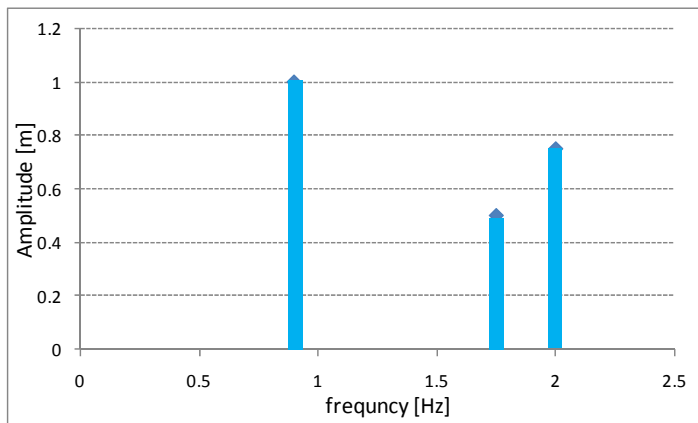


Figure 2-5 : Amplitude versus Frequency as Result from Fourier Transform

If all information from the Fourier transform is available, a new sum of harmonic waves can be created at the exact configuration as before.

2.3.2 Fast Fourier Transform (FFT)

The Fast Fourier Transform (FFT) is another way to translate the times series wave signal into frequency domain and is commonly used compare to Fourier transform. The FFT plots power spectral density over frequency which is more useful for engineers. This spectrum will be discussed in depth at section 2.4.2.

Power spectral density or spectrum can be reversed to a time series wave by assuming that the phase angle is distributed randomly. This is called Inverse Fast Fourier Transform (IFFT). However, this method could not create the exact copy of time series wave that spectrum was created. In addition, this spectrum has wider range possibility of time series waves. A complete FFT formulation can be found at [41].

2.4 Hydrodynamics

The motion of the water or hydrodynamics is caused by velocity and acceleration of the water particles. These components are normally seen as current and wave in the ocean and acting as loads to the MCT. As the MCT is exposed to both aspects, therefore it will be discussed in this section.

2.4.1 Current Description

Currents are driven by tides, ocean circulation, river flow, temperature different, salinity and storm surge. The velocity produced by these sources are varies in space and time. The length and timescale of the variation in current velocity are much larger compare to the associate loadings in the design of MCT, therefore, it is assumed that the surface current velocity and direction to be constant in the design calculations.

In this thesis, the current model for MCT design is defined by a simple current profile over depth with the power law profile taken from [1] and expressed in equation (2-5).

$$U_c(z) = U_{c0} \left(\frac{z+d}{d} \right)^{\frac{1}{7}} \quad (-d \leq z \leq 0) \quad (2-5)$$

Where	$U_c(z)$	=	current velocity at elevation z	[m/s]
	U_{c0}	=	current velocity at sea surface ($z = 0$)	[m/s]
	z	=	vertical coordinate, positive upward from MSL	[m]
	d	=	mean water depth	[m]

2.4.2 Wave Description

The wave climate at specific location is described as statistical parameters of random process that remain constant (stationary) for every 3 hours. This characteristic is called seastate and can be plotted as power density spectra or spectrum in short through FFT.

Two commonly used spectrums are:

- Pierson-Moskowitz (PM) wave spectrum, for fully developed seas
- JONSWAP wave spectrum, for fetch limited wind generated seas

Figure 2-6 shows the PM and JONSWAP wave spectra. Both spectra are derived from significant wave height (H_s) and mean zero-crossing wave period (T_z).

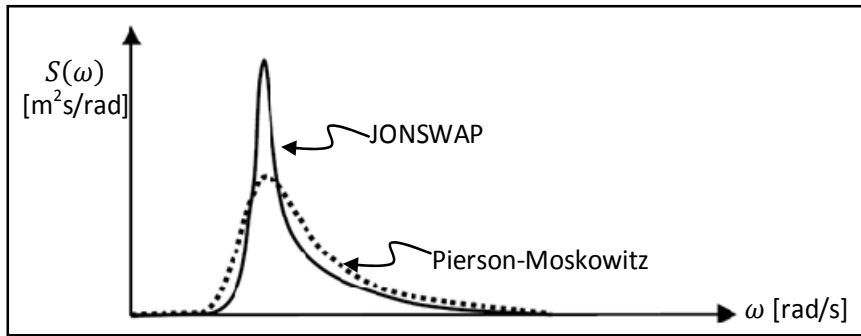


Figure 2-6 : JONSWAP and Pierson-Moskowitz Wave Spectra

Pierson-Moskowitz spectrum can be expressed by equation (2-6):

$$S_{PM}(\omega) = \frac{A}{\omega^5} \exp\left\{-\frac{B}{\omega^4}\right\}$$

$$A = \frac{4\pi^3 H_s^2}{T_z^4} \text{ and } B = \frac{16\pi^3}{T_z^4} \quad (2-6)$$

Where $S_{PM}(\omega)$ = Pierson-Moskowitz variance density spectrum [m²s]
 ω = angular frequency [rad/s]
 H_s = significant wave height [m]
 T_z = mean zero wave-crossing period [s]

JONSWAP spectrum is based on measurement from the North Sea at Joint North Sea Wave Project (JONSWAP) in 1968 and 1969. It has the shape of PM spectrum with enhancement modification at the peak.

JONSWAP spectrum can be expressed by equation (2-7):

$$S_{JS}(\omega) = nf \cdot \frac{A}{\omega^5} \exp\left\{-\frac{B}{\omega^4}\right\} \cdot \left\{ \gamma \exp\left\{-\frac{1}{2}\left(\frac{\omega-\omega_m}{\sigma\omega_m}\right)^2\right\} \right\}$$

$$\omega_m = \left(\frac{4}{5}B\right)^{\frac{1}{4}} \quad (2-7)$$

Where $S_{JS}(\omega)$ = JONSWAP variance density spectrum [m²s]
 nf = normalizing factor JONSWAP and PM spectrum [-]
 γ = peak shape parameter ($\gamma = 3.3$) [-]
 ω_m = modal angular frequency [rad/s]
 σ = numerical parameter [-]
 $\sigma_a = 0.07$ ($\sigma = \sigma_a$ for $\omega < \omega_m$) [-]
 $\sigma_b = 0.09$ ($\sigma = \sigma_b$ for $\omega \geq \omega_m$) [-]

The average value for γ , σ_a and σ_b were taken from measurement of the Joint North Sea Wave Project. The offshore group at the Delft University of Technology found a normalizing factor of:

$$nf = 0.625 \text{ (for } \gamma = 3.3 \text{)} \quad [-]$$

With the parameters given above, the JONSWAP spectrum can be expressed by H_s and T_z at equation (2-8).

$$S_{JS}(\omega) = 2.5\pi^3 \cdot \frac{H_s^2}{T_z^4 \omega^5} \exp\left\{-\frac{16\pi^3}{T_z^4 \omega^4}\right\} \cdot \left\{3.3 \exp\left\{-\frac{1}{2}\left(\frac{\omega-\omega_n}{\sigma\omega_n}\right)^2\right\}\right\}$$

$$\omega_m = \left(12.8 \cdot \frac{\pi^3}{T_z^4}\right)^{\frac{1}{4}} \quad (2-8)$$

With the appropriate spectrum, IFFT can be performed to create regular sinusoid waves. These harmonic waves are translated into velocity and acceleration for load calculation through linear wave theory of Airy [22]. The horizontal water particle kinematics is expressed by equation (2-9).

$$u_w(z, t) = \zeta_a \cdot \omega \cdot \frac{\cosh k(z+d)}{\sinh kd} \cdot \cos(\omega t + \varphi)$$

$$\dot{u}_w(z, t) = \zeta_a \cdot \omega^2 \cdot \frac{\cosh k(z+d)}{\sinh kd} \cdot \sin(\omega t + \varphi) \quad (2-9)$$

Where $u_w(z, t)$ =	wave horizontal water particle velocity	[m/s]
$\dot{u}_w(z, t)$ =	wave horizontal water particle acceleration	[m/s ²]
ζ_a =	wave amplitude ($\zeta_a = \frac{1}{2}H$)	[m]
k =	wave number ($k = 2\pi/\lambda$)	[rad/m]
z =	vertical coordinate, positive upward from MSL	[m]
d =	mean water depth	[m]
λ =	wave length ($\lambda = \frac{g}{2\pi} T^2 \tanh \frac{2\pi d}{\lambda}$)	[m]
g =	acceleration of gravity	[m/s ²]
H =	wave height	[m]

2.4.3 Hydrodynamic Loads on Pile

As mentioned earlier, velocities and accelerations of water particles cause hydrodynamic loads in the structure. For slender piles, the loading are described by Morison equation as

expressed by equation (2-10). It named after J.R Morison who derived the formulation in 1950. Morison formulae cover the total hydrodynamic loads from drag and inertia.

$$\begin{aligned}
 q_{hydro} &= f_i + f_d \\
 &= \frac{\pi}{4} \rho_w C_M D^2 \cdot \dot{u} + \frac{1}{2} \rho_w C_D D \cdot |u|u
 \end{aligned}
 \tag{2-10}$$

Where q_{hydro}	= hydrodynamic load per unit length	[N/m]
f_i	= hydrodynamic inertia load per unit length	[N/m]
f_d	= hydrodynamic drag load per unit length	[N/m]
C_M	= inertia coefficient	[-]
C_D	= drag coefficient	[-]
D	= diameter of pile	[m]
ρ_w	= mass density of water	[kg/m ³]
\dot{u}	= horizontal water particle acceleration	[m/s ²]
u	= horizontal water particle velocity	[m/s]

The Morison equation is based on experiments, therefore the inertia and drag coefficient are found in many variety. For tubular members, the following drag and inertia wave force coefficients should be used as per API RP 2A:

$$C_D = 0.8 \text{ for rough members} \quad C_D = 0.5 \text{ for smooth members} \quad C_M = 2.0$$

The horizontal particle velocity for loading calculation depends on current, wave and the motion of the structure. Therefore equation (2-11) accounts the relative aspects of the velocity acting on structure.

$$u_r(z, t) = U_c(z) + u_w(z, t) - u_s(z, t) \tag{2-11}$$

Where $u_r(z, t)$	= relative velocity of water to structure	[m/s]
$U_c(z)$	= current velocity	[m/s]
$u_w(z, t)$	= wave horizontal water particle velocity	[m/s]
$u_s(z, t)$	= structure horizontal velocity	[m/s]

The equation (2-10) can be rewritten due to the total motion in the structure at (2-12).

$$q_{hydro} = \frac{\pi}{4} \rho_w C_M D^2 \cdot \dot{u}_w - \frac{\pi}{4} \rho_w (C_M - 1) D^2 \cdot \dot{u}_s + \frac{1}{2} \rho_w C_D D \cdot |u_r|u_r
 \tag{2-12}$$

2.4.4 Hydrodynamic Loads on Turbine

The hydrodynamic loads on turbine are defined by three theories; momentum, blade element and blade element momentum theory. Each theory will be discussed in depth at the following sections.

2.4.4.1 Momentum Theory

The momentum theory is taken from basic conservation law of fluid mechanics to the rotor and water flow as a whole to estimate the rotor performance. In this case, one dimensional momentum theory is considered to determine the axial force of water flow on turbine (D_{ax})

As the water flows to the rotor, the velocity decreases. The modelling of water flow through an infinitely thin permeable rotor which is called actuator disk can be seen in Figure 2-7.

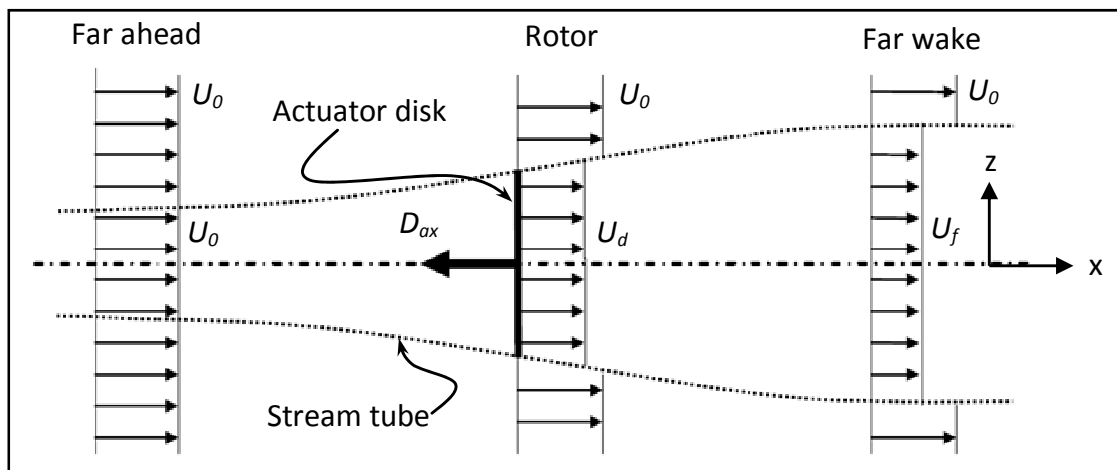


Figure 2-7 : Actuator Disk Model

Within the boundary layer, an induction factor (a) is introduced to measure the actual velocity at the rotor as expressed by equation (2-13). Laws of conservation of mass and Bernoulli enable the stream velocity in the far wake to be derived [2].

$$U_d = U_0 \cdot (1 - a) \text{ and } U_f = U_0 \cdot (1 - 2a)$$

$$a = \frac{U_0 - U_d}{U_0} \tag{2-13}$$

Where	U_0	= undisturbed stream velocity	[m/s]
	U_d	= stream velocity at the actuator disk	[m/s]
	U_f	= stream velocity at far wake	[m/s]
	a	= induction factor	[-]

The stream tube enclosing the flow through the actuator disk has a constant mass flow rate at all cross sections from far ahead to far awake. The mass flow at the actuator disk is driven by the static pressure as seen in Figure 2-8. The acting load on disk can be derived from the pressure difference in the rotor and can be expressed by equation (2-14).

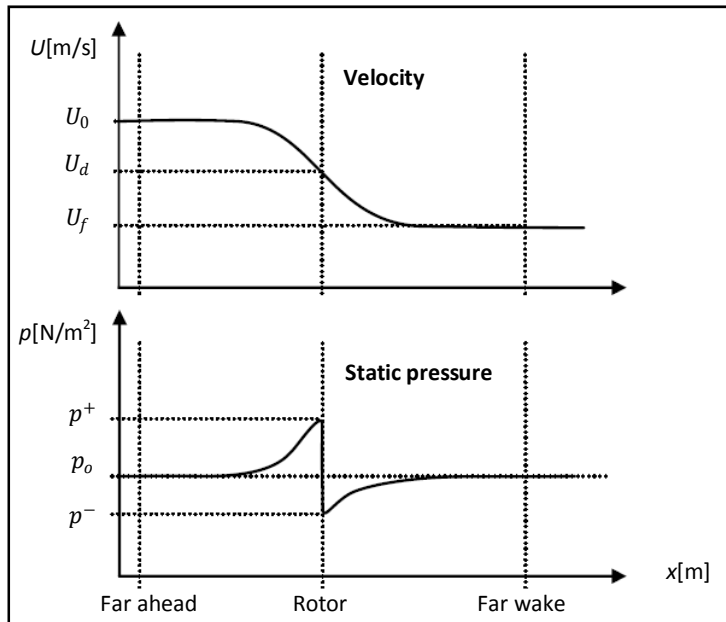


Figure 2-8 : Velocity and Static Pressure along the Stream Line

$$D_{ax} = A_d \cdot (p^+ - p^-) \quad (2-14)$$

- Where
- D_{ax} = axial force [N]
 - A_d = surface area of the actuator disk ($A_d = \pi R^2$) [m²]
 - p^+ = pressure on the upstream side of the actuator [N/m²]
 - p^- = pressure on the downstream side of the actuator [N/m²]
 - R = radius of rotor [m]

According to Bernoulli's law, the total pressure stays constant along the stream line if there is no power loss present. Thus, the equation (2-15) can be derived to find the axial force.

$$p_o + \frac{1}{2} \rho_w U_0^2 = p^+ + \frac{1}{2} \rho_w U_d^2 \quad \text{for the leftside of the actuator disk}$$

$$p^- + \frac{1}{2} \rho_w U_d^2 = p_o + \frac{1}{2} \rho_w U_f^2 \quad \text{for the rightside of the actuator disk}$$

(2-15)

- Where
- p_o = undisturbed atmospheric pressure [N/m²]
 - ρ_w = mass density of water [kg/m³]

The axial force can be extracted by substituting equation (2-14) and (2-15) as shown in equation (2-16).

$$D_{ax} = A_d \cdot \frac{1}{2} \cdot \rho_w \cdot U_0^2 \cdot 4a(1 - a) \tag{2-16}$$

The axial force can also be expressed into dimensionless axial force coefficient by equation (2-17).

$$C_{Dax} = \frac{D_{ax}}{F_C} = \frac{A_d \cdot \frac{1}{2} \cdot \rho_w \cdot U_0^2 \cdot 4a(1 - a)}{A_d \cdot \frac{1}{2} \cdot \rho_w \cdot U_0^2} = 4a(1 - a) \tag{2-17}$$

Where C_{Dax} = axial force coefficient [-]
 F_C = undisturbed current force [N]

Equation (2-17) describes the relationship between undisturbed current force, axial coefficient and the induction factor. However, the induction factor remains unknown. The blade element theory on section 2.4.4.2 provides the alternative to find the axial force coefficient which involves the induction factor.

2.4.4.2 Blade Element Theory

The blade element theory assumed that the blade is divided into small elements with constant cross sections as shown in Figure 2-9. From the cross section, two-dimensional analysis is made with assumptions:

- No hydrodynamic interaction between elements
- The lift and drag forces are the only load acting on the hydrofoil

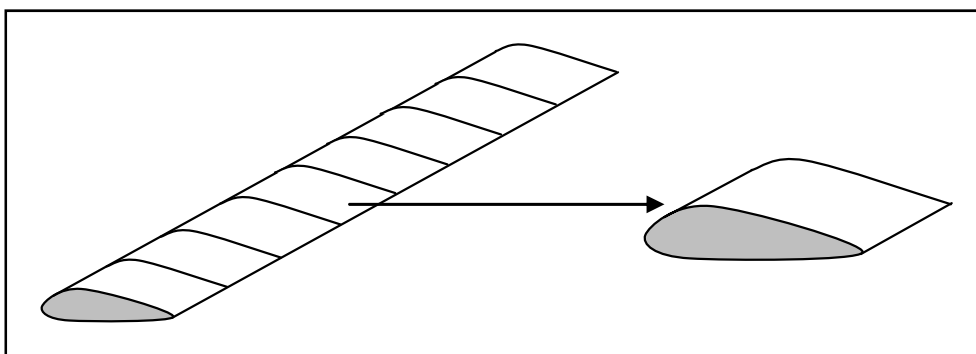


Figure 2-9 : Elements of a Blade

The lift and drag forces are caused by stream velocity at the rotor and the rotor tangential velocity as expressed in equation (2-18) and illustrated by Figure 2-10.

$$U_d = U_0 \cdot (1 - a)$$

$$U_t = \Omega \cdot r$$

(2-18)

Where	U_d	=	stream velocity at the rotor plane	[m/s]
	U_t	=	rotor tangential velocity	[m/s]
	U_0	=	undisturbed stream velocity	[m/s]
	a	=	induction factor	[-]
	Ω	=	rotor angular velocity	[rad/s]
	r	=	radial position of the element	[m]

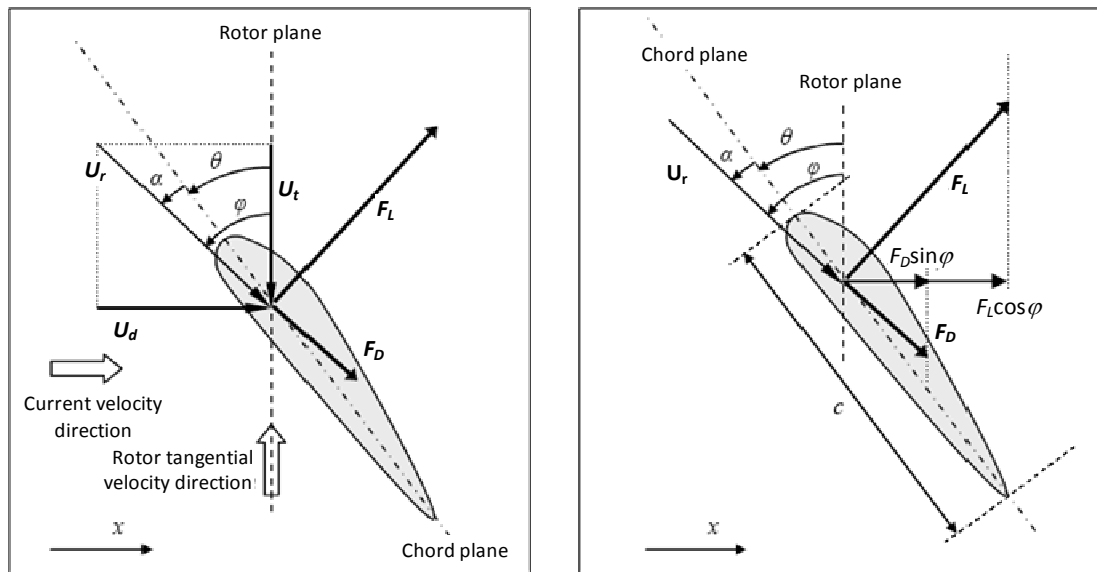

Figure 2-10 : Velocity and Load on Blade Element

Figure 2-10 shows the velocity vector acting on hydrofoil cross section which causes the lift and drag forces. The resultant of the current and rotor tangential velocity creates the drag force and lift force as expressed by equation (2-19).

$$F_L = \frac{1}{2} \cdot C_L(\alpha) \cdot \rho_w \cdot U_r^2 \cdot c \cdot \Delta r$$

$$F_D = \frac{1}{2} \cdot C_D(\alpha) \cdot \rho_w \cdot U_r^2 \cdot c \cdot \Delta r \quad \text{and} \quad U_r = \sqrt{U_d^2 + U_t^2}$$

(2-19)

Where	F_L	=	lift force	[N]
	$C_L(\alpha)$	=	lift coefficient	[-]
	F_D	=	drag force	[N]
	$C_D(\alpha)$	=	drag coefficient	[-]
	U_r	=	resultant of current and rotor tangential velocity	[m/s]
	c	=	hydrofoil chord length	[m]

Δr = radial length of blade element [m]
 α = angle of attack [deg]

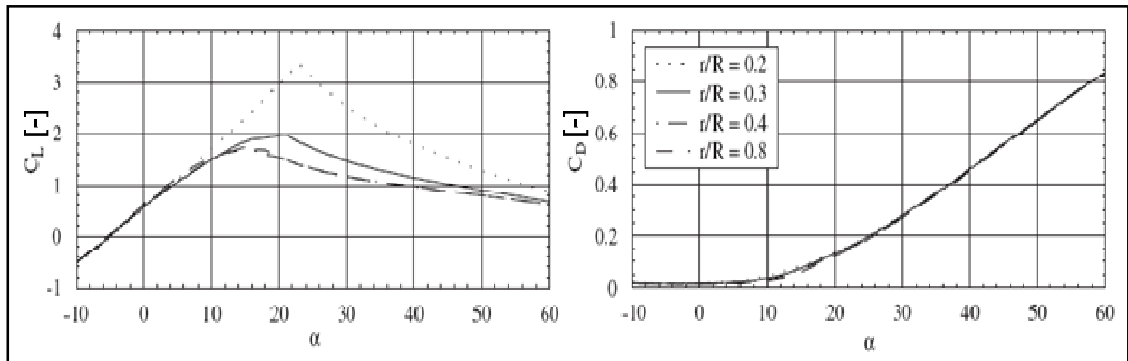


Figure 2-11 : Lift and Drag Coefficient over Angle of Attack (Batten, 2006)

The forces are affected by the lift and drag coefficients which are influenced by angle of attack and the shape of hydrofoil. Figure 2-11 shows the lift and drag coefficient for a typical hydrofoil over angle of attack. At certain value of α , between 15 and 25, the lift coefficient reaches its peak and then decrease while the drag coefficient keeps increasing. It means that the power generation will reach its peak and then decrease while the acting force on MCT keeps increasing following the shape of lift and drag coefficient respectively.

The resulting force F_x on an element in x-direction can be calculated as follows:

$$\alpha = \varphi - \theta$$

$$\varphi = \frac{360}{2\pi} \cdot \arctan\left(\frac{U_d}{U_t}\right)$$

$$F_x = F_L \cos \varphi + F_D \sin \varphi$$

(2-20)

Where φ = angle of inflow [deg]
 θ = pitch angle [deg]
 F_x = element force on x-axis [N]

For number of elements N_s and number of blades N_b in a rotor, the axial force in the rotor shaft can be expressed by equation (2-21).

$$D_{ax} = N_b \cdot \sum_{i=1}^{N_s} F_{x,i}$$

(2-21)

Where N_s = number of blades in a rotor [-]
 N_b = number of elements in a blade [-]
 $F_{x,i}$ = resulting force on x-axis at element i [N]

The axial force coefficient using blade element theory now can be derived by equation (2-22).

$$C_{Dax} = \frac{D_{ax}}{F_C} = \frac{N_b \cdot \sum_{i=1}^{N_s} F_{x,i}}{A_d \cdot \frac{1}{2} \cdot \rho_w \cdot U_0^2} \quad (2-22)$$

Where C_{Dax} = axial force coefficient [-]
 F_C = undisturbed current force [N]

To be note that the axial coefficient depends on induction factor as it was used in equation (2-17) and remains unknown. In the next section, both momentum and blade element theories will be combined to determine the induction factor as well as the axial force.

2.4.4.3 Blade Element Momentum Theory

The blade element momentum (BEM) theory combines the momentum theory and the blade element theory to determine the axial force acting on turbine. According to BEM theory, the axial coefficients from momentum and blade element theories are equal as expressed in equation (2-23). Both coefficients are induction factor dependent which now can be calculated. It appears at range of 0 and 0.5 for no current velocity decrease at actuator disk and velocity in far wake becomes zero respectively.

$$C_{Dax,M} = C_{Dax,BE} \quad (2-23)$$

Where $C_{Dax,M}$ = axial force coefficient from momentum theory [-]
 $C_{Dax,BE}$ = axial force coefficient from blade element theory [-]

Once the induction factor has been found, the hydrodynamic axial force on turbine can be determined by equation (2-24).

$$D_{ax} = C_{Dax} \cdot F_C = C_{Dax} \cdot A_d \cdot \frac{1}{2} \cdot \rho_w \cdot U_0^2 \quad (2-24)$$

2.5 Turbine Description

Many arrangements arrived in the marine current energy converter such as horizontal axis turbine, vertical axis turbine, hydrofoil device and venturi devices. The horizontal axis turbine has been developed in advance on wind energy converter, which gives more advantages compare to other devices. With the same mechanism of wind energy extraction, the horizontal axis turbine presently is being desired in current energy development and therefore will be used and discussed further in this thesis.

Unlike the wind turbine that has its own market and brand, the horizontal axis MCT currently is at a prototype stage, where single devices are placed at isolated testing site. Therefore the MCT selection will be based on assumption and developed from wind turbine as well as MCT most recent research.

2.5.1 Power Capture

Power capture of MCT is the main topic for tidal power generation. As the current stream flows through the blades and drives the blades into a certain tip speed, thus, power is generated. The maximum power generation is created at a certain blade rotational speed which influences the fatigue design.

Figure 2-12 shows the basic concept of wind turbine power generation which applies for MCT. The power capacity of a single turbine is formulated in equation (2-25). However, the power coefficient varies from papers and publications. From Fraenkel (1999), MCT had power coefficient between 0.35-0.5. Mellor (2004), C_p varies by the flow velocity. It could reach 0.4-0.45 at maximum flow between 1.75 to 3.5 m/s. Thake (2005) took the result from SeaFlow Project with $C_p \approx 0.4$. Blunden & Bahaj (2006) got $C_p = 0.3$ taken from typically 15m turbine diameter that could produce 300 kW average power.

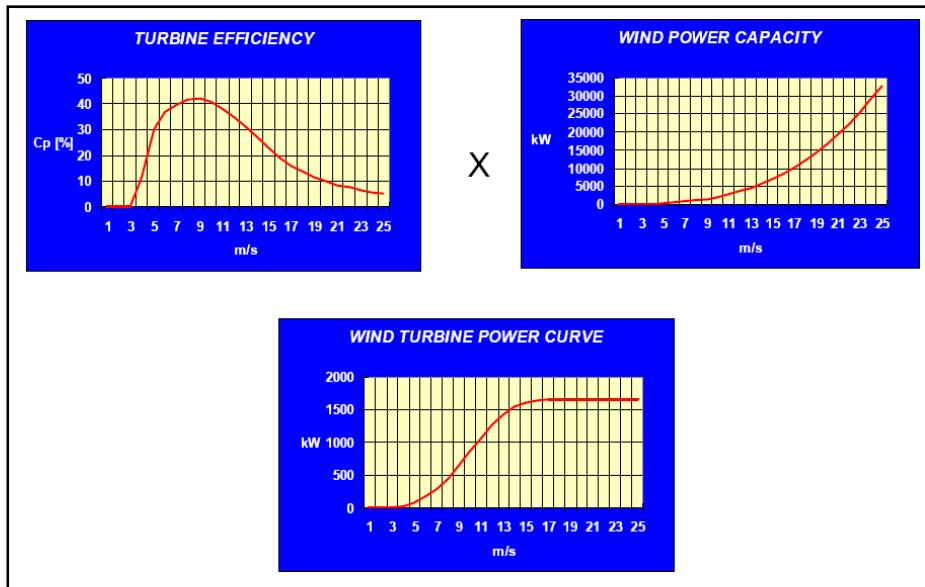


Figure 2-12 : Wind Turbine Power Curve (Shell, 2010)

$$P = C_p \cdot \rho_w \cdot A_d \cdot U_c^3 \tag{2-25}$$

Where P = power capacity [Watt]
 C_p = power coefficient [-]
 ρ_w = mass density of water [kg/m³]

A_d = surface area of actuator disc [m²]

U_c = current velocity [m/s]

The power coefficient is influenced by the ratio between speed of the blade tip and current speed as plotted in Figure 2-13. The curve shows peak for this particular blade at approximately 5 and 6 of *TSR*. To capture the maximum power at every current speed, the *TSR* should be changed accordingly to suit the C_p -*TSR* curve at its maximum value.

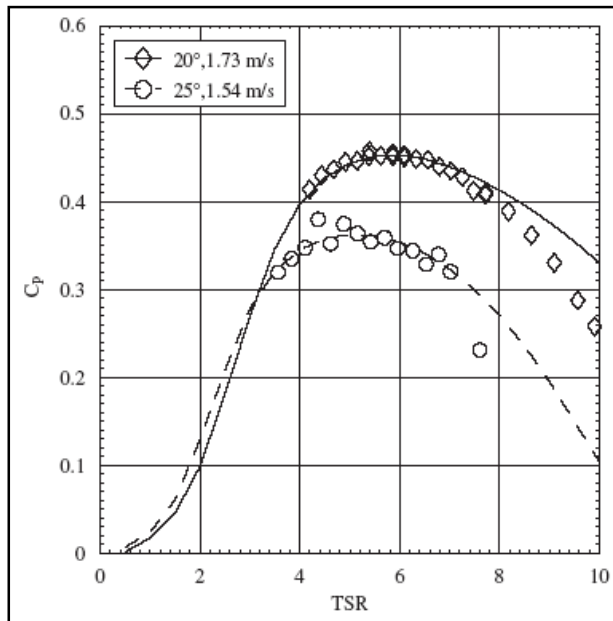


Figure 2-13 : Power Coefficient versus Tip Speed Ratio (Batten, 2006)

$$TSR = \frac{U_{tip}}{U_0} = \frac{\Omega R}{U_0} \quad (2-26)$$

Where TSR = tip speed ratio [m/s]

U_{tip} = blade tip speed [m/s]

U_0 = undisturbed stream velocity [m/s]

Ω = rotor angular velocity [rad/s]

R = blade radius [m]

2.5.2 Variable vs. Constant Speed Rotor

One constant rotational speed value can produce the maximum amount of power at any different current velocity. On the other hand, for variable speed rotor, a turbine can reach optimum rotational speed at each current velocity. Figure 2-14 shows the difference between variable and constant speed rotor for a wind turbine power production. Each curve plots the power production against rotational speed at specific wind speed; power

production reaches its maximum at certain rotational speed due to stall (section 2.5.3). The red curved line expresses the optimum power production for a turbine at different wind speed, while the blue vertical line shows the production for a constant speed rotor operating at 27 RPM for the same turbine. It can be concluded that variable speed rotor gives more advantages compare to constant speed rotor in the power production. However, for simplification in fatigue analysis, the constant speed rotor is considered in this thesis.

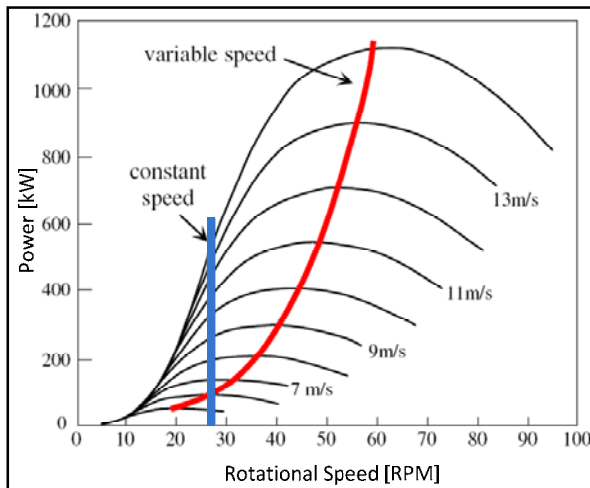


Figure 2-14 : Power vs. Rotational Speed at Different Wind Velocities (Pijpaert, T., 2002)

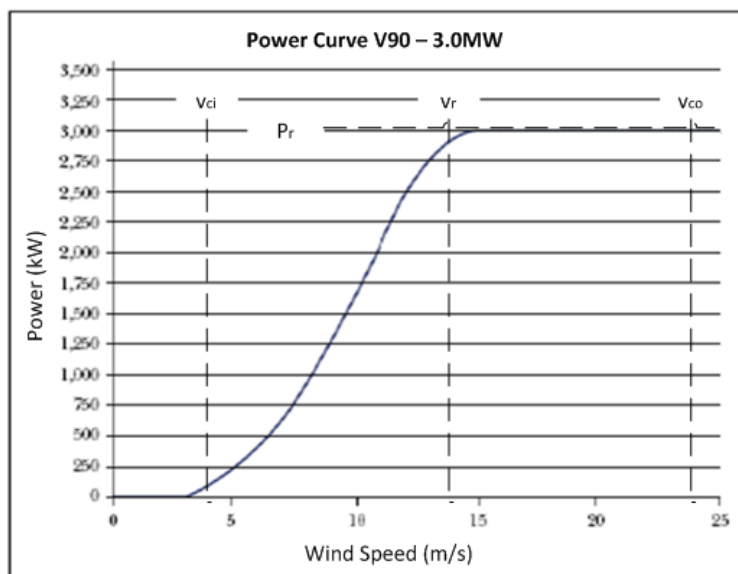


Figure 2-15 : Power versus Wind Velocity V90-3.0MW (DUWIND)

The V90-3.0MW wind turbine power out-put of variable speed rotor at different wind speed velocity is plotted in Figure 2-15. It implies the three characteristics of governing velocity to generate power production.

P_r = Rated power, maximum allowable converted power

v_{ci} = Cut-in speed, initial speed which the turbine starts operating

v_r = Rated/nominal speed, the lowest speed which P_r is reached

v_{co} = Cut-out speed, the maximum speed which operations are stopped.

The speed characteristic defines four different intervals for turbine operation. Below cut-in speed, no power will be generated due to mechanical friction is higher than incoming energy. Between cut-in and rated speed, maximum power is generated according to the occurring speed. At the rated speed, the generator reaches the maximum power to be converted. Above this speed, there will be an excessive power production which could damage the generator. As the ideal condition is to keep the power at constant value of P_r , therefore, stall of pitch regulation is applied as power control. At last, above the cut-out speed, no power will be generated in order to prevent extreme loading.

2.5.3 Stall vs. Pitch Regulated Power Control

Two techniques have been developed in order to control turbine power generation once the occurring speed exceeded the rated speed. Stall regulated power control mostly can be found in constant speed rotor, while variable speed rotor are commonly used pitch regulated.

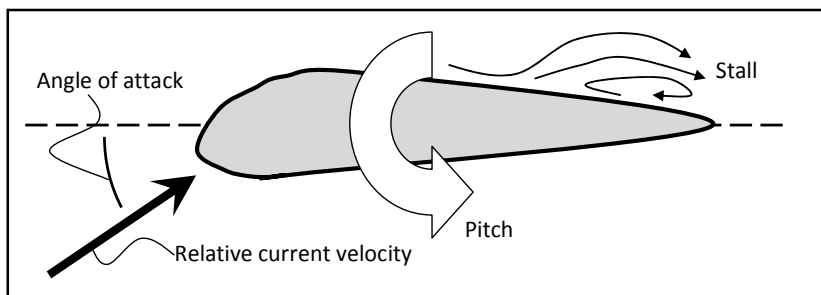


Figure 2-16 : Stall and Pitch on a Hydrofoil

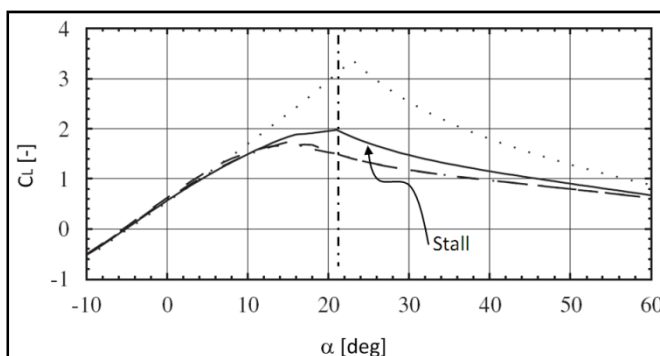


Figure 2-17 : Lift Coefficient versus Angle of Attack (Batten, 2006)

Stall is a phenomenon of stream line separation between current and surface of hydrofoil as shown in Figure 2-16. The separation occurs above a certain angle of attack which leads to a turbulence and causes decrement of lift force. Decrement in lift with increasing angle of

attack can be set as definition of stall (Corten, 2001) as shown in Figure 2-17. When current velocity increases at a constant rotor speed, the angle of attack will increase; and at a certain current velocity, the blades will begin to stall. This will cause decrement in lift but on the other hand the drag will keep on increasing. At this point, there will be no power increment even with higher current velocity. The stall regulated system is the simplest technique, since it fixed to the hub and cannot be pitched.

Pitch regulated power control enables the blades rotating at its longitudinal axis therefore the angle of attack can be changed simultaneously. Increment in pitch decreases angle of attack and decrement angle of attack reduces lift coefficient as shown Figure 2-16 and Figure 2-17 respectively. This phenomenon will decrease the power generation as well. Thus, when the rated power is achieved and the current speed rises above the rated speed, the power can be kept constant at rated power value through a pitch adjustment. It is also possible to reduce power generation by pitching the blades at opposite direction which increases the angle of attack. This technique is called active stall regulated power control.

2.6 Dynamics of Marine Current Turbine

The MCT is exposed to the dynamically changing loads. This section will describe the basic of equation of motion followed by harmonic excitation from turbine and wave as well as the hydrodynamic damping as the effect of rotating blades.

2.6.1 Equation of Motion

The dynamics of MCT can be modelled as numbers of coupled multi degree-of-freedom (DOF) mass-damper-spring system. The simple equation of motion with 1-DOF can be expressed by equation (2-27) and illustrated in Figure 2-18.

$$m\ddot{u}(t) + c\dot{u}(t) + ku(t) = F(t) \tag{2-27}$$

Where	m	=	mass	[kg]
	c	=	damping coefficient	[Ns/m]
	k	=	spring constant	[N/m]
	$\ddot{u}(t)$	=	body acceleration	[m/s ²]
	$\dot{u}(t)$	=	body velocity	[m/s]
	$u(t)$	=	body displacement	[m]
	$F(t)$	=	harmonic excitation	[N]

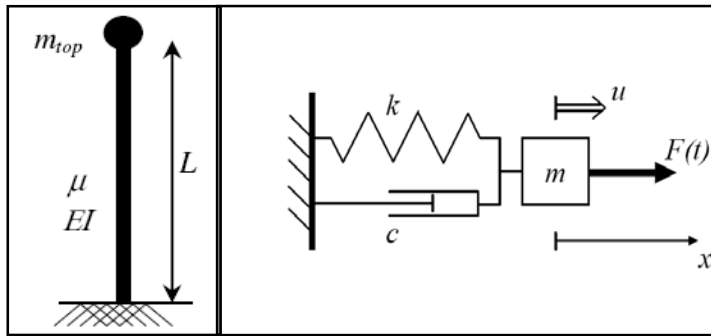


Figure 2-18 : 1-DOF mass-damper-spring system

When the harmonic excitation is applied to the MCT, three steady state responses can be distinguished according to frequency of excitation (f_e) over natural frequency of the structure (f_n). Figure 2-19 illustrates the steady state of structure responses based on Dynamic Amplification Factor (DAF) over normalized frequency (f_e/f_n). For quasi-static range, the structure response follows the excitation response as observed with DAF near to 1. Next at resonance, the DAF reaches its maximum which can cause the failure of the structure this range should be avoided at the design of MCT. Last, the inertia-dominated range shows mass of structure is dominating the excitation force, therefore the DAF decreases accordingly.

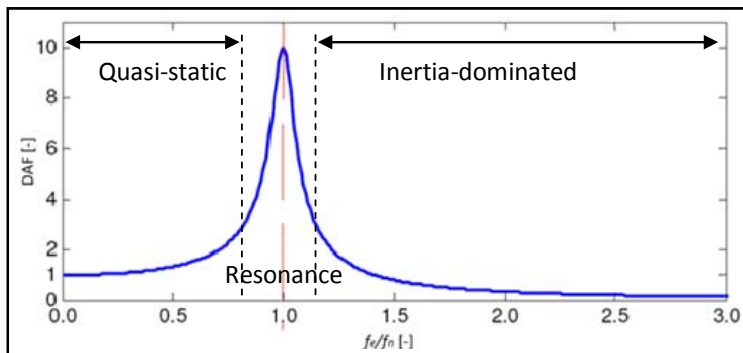


Figure 2-19 : DAF versus Normalized Frequency

The first mode of structure natural frequency can be expressed by equation (2-32), assuming that the model consists of a uniform beam with a top mass and a fixed base as shown in Figure 2-18 [38].

$$f_n^2 \cong \frac{3.04}{4\pi^2} \frac{EI}{(m_{top} + 0.227\mu L)L^3} \tag{2-28}$$

- Where f_n = natural frequency of structure [Hz]
- m_{top} = mass in the top of tower [kg]
- μ = mass per meter of tower [kg/m]

L = height of tower [m]

EI = bending stiffness of tower [Nm²]

By using parameters in (2-29), equation (2-28) can be re-written as follows,

$$I \cong \frac{1}{8} \pi D_{av}^3 t_w, \quad \mu = \rho_s \pi D_{av} t_w \quad \text{and} \quad a = \frac{m_{top}}{\rho_s \pi D_{av} t_w L} \quad (2-29)$$

$$f_n^2 \cong \frac{D_{av}}{L^2} \sqrt{\frac{E}{104(a + 0.227)\rho_s}} \quad (2-30)$$

Where t_w = wall thickness of tower [m]

D_{av} = average diameter of tower ($=D - t_w$) [m]

ρ_s = density of steel ($=7850$) [kg/m³]

E = young's modulus ($=2.10^8$) [kN/m²]

2.6.2 Harmonic Excitation of the Turbine

The source of harmonic excitation is coming from wave and turbine. The excitation from turbine can be seen easily. The rotor's rotational frequency called 1P is the first excitation frequency on structure. The second excitation frequency is coming from the blade and depends on the number of blades; for 3-bladed turbine, it called 3P. Figure 2-20 describes the range of 1P and 3P excitation of 3-bladed turbine with a rotational speed ranging from 10.5 to 24.5 RPM.

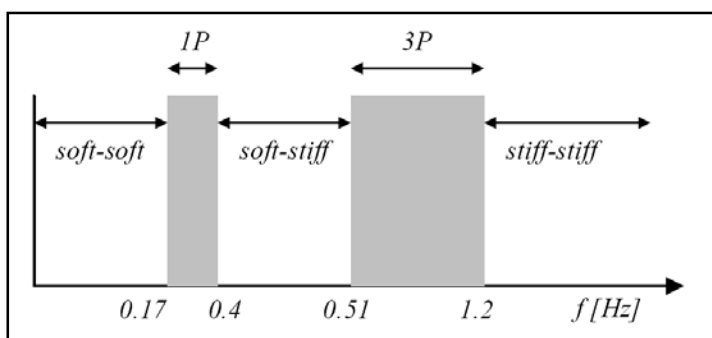


Figure 2-20 : Excitation Frequency of 1P and 3P Turbine [28]

The diameter of rotor also gives influence in the excitation frequency as expressed by equation (2-31) which is extracted from tip speed ratio at equation (2-26). For a constant TSR at certain stream velocity, the f_{1P} will decrease as the diameter of rotor increase. The increment in diameter requires higher tower hub. Consequently, the natural period of structure will decrease as stated in equation (2-30).

$$\text{as, } \Omega = 2\pi f_{1P} \text{ thus, } f_{1P} = \frac{TSR \cdot U_0}{\pi D_R} \quad (2-31)$$

Where f_{1P} = rotor's rotational frequency [Hz]
 D_R = diameter of rotor [m]

It is important to keep the natural frequency of structure outside the range of the turbine's frequency bands in order to avoid resonance which causes failure of the structure. Figure 2-20 defines the outside ranges of turbine harmonic excitation and are categorized as follows:

- Soft-soft : structure natural frequency below rotor's rotational frequency
- Soft-stiff : structure natural frequency between the rotor's rotational frequency and blade passing frequency
- Stiff-stiff : structure natural frequency above the blade passing frequency

The soft-soft band is more attractive compare to other bands because it requires less material and thus economically suitable. However, the structural response to fatigue failure is more sensitive as the wave bands normally appear at low frequency.

2.6.3 Harmonic Excitation of the Wave

For offshore structures the harmonic excitation from wave generally has lower frequency compare to the turbine. That is because the waves come from various periods and spread out in the frequency band.

Since the MCT is designed using soft-soft range, it becomes prone to wave excitation. Figure 2-21 illustrates the occurrence of wave frequency in accordance with 1P and 3P frequencies of the turbine. As seen in the figure, approximately 10% of the wave occurrence could cause resonance in the structure. Therefore, a hydrodynamic damping is needed to reduce the dynamic amplification on the structure response.

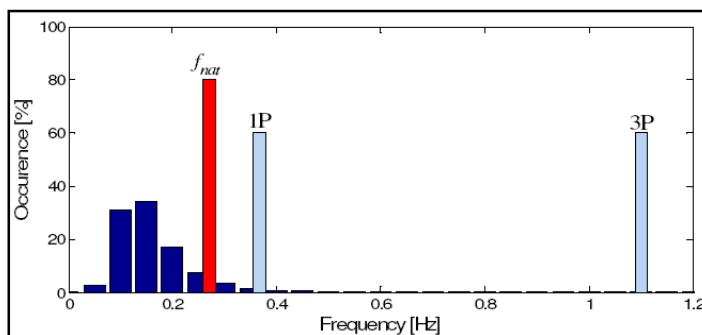


Figure 2-21 : Occurrence of Wave Frequency with 1P and 3P Frequencies [38]

2.6.4 Hydrodynamic Damping

When an operating turbine moves against the stream, the blades experience an increasing load as a result of an increasing stream velocity. This load is acting against the tower top motion. Analogous for backward movement, it reduces the loading as well as the motion in the top of tower. This condition is known as hydrodynamic damping.

The hydrodynamic damping due to rotor is modelled into two conditions, low damping of 1.5% in case the turbine is not operating and high damping (5%) for turbine in operation. This estimation is taken from offshore wind turbine energy [28].

Based on API RP2A, for typical pile founded tubular space frame substructures, a total damping value of 2% of critical is appropriate. This accounts for all sources of damping including structural, foundation and hydrodynamic effects.

As an engineering judgement, 4% of hydrodynamic damping at operational condition and 2% for non-operating turbine will be considered in this thesis.

2.7 Foundation

The soil is assumed to absorb the associate loadings on MCT. Thus, pile-soil interaction should be correctly represented in the model. The foundation can be modelled by rotational and translational spring or by clamping at a certain depth as shown in Figure 2-22.

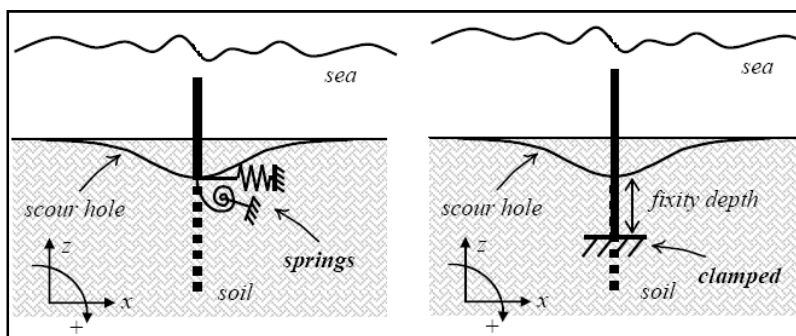


Figure 2-22 : Pile-Soil Interaction Foundation Model

Equation (2-32) shows the spring foundation model which gives the rotation and horizontal translation affected by horizontal force and bending moment at working points. This model requires advance analysis and data of the soil which is appropriate for detailed engineering phase.

$$K \cdot \underline{u} = \underline{F}$$

$$\begin{bmatrix} k_{11} & k_{21} \\ k_{12} & k_{22} \end{bmatrix} \begin{bmatrix} u \\ \varphi \end{bmatrix} = \begin{bmatrix} F \\ M \end{bmatrix}$$

(2-32)

Where	K	= stiffness matrix	[-]
	\underline{u}	= displacement vector	[-]
	\underline{F}	= load vector	[-]
	k_{ij}	= spring constant	[-]
	u	= horizontal displacement	[m]
	φ	= rotation	[rad]
	F	= horizontal load	[N]
	M	= bending moment	[Nm]

For clamped foundation model, the horizontal displacement and rotation remains zero at the clamped joint as expressed in equation (2-33). This joint is called the *fixity depth*. Table 2-1 shows the variety of fixity depth at different soil types with D indicates the pile diameter.

$$K = \begin{bmatrix} \infty & 0 \\ 0 & \infty \end{bmatrix} \tag{2-33}$$

Table 2-1 : Fixity Depth of Different Types of Soil [4]

Soil Type	Fixity Depth
Stiff Clays	3.5 D - 4.5 D
Very Soft Silts	7 D - 8 D
General Calculations	6 D

The clamped foundation model has been selected in this thesis due to unavailability of pile-soil interaction data.

2.8 Limit State Design

A limit state is a set of performance criteria that must be met when the structure exposed to incoming loads. Limit state design (LSD) is a modernization design method used in structural design. It combines the statistical factored design of loading on the structure and the material of the structure into an acceptable safety level.

The safety level of structure requires two principle criteria, which are Ultimate Limit State (ULS) and Serviceability Limit State (SLS). Nevertheless, other criteria have the same importance level of safety at certain condition such as Accidental Limit State (ALS) and Fatigue Limit State (FLS).

2.8.1 Ultimate Limit State

The structure must withstand when exposed to extreme design load. Bending moment, shear stress and axial stress are the parameters to be considered. The structure is stated to

be safe when the factored magnified loadings are less than the factored reduced resistance of the material.

2.8.2 Service Limit State

The structure must remain functioned as intended when subjected to daily routine loadings. The main purpose of SLS is to ensure that personnel in the structure are not unnerved by large deflection on the floor. Since the MCT is designed to be unmanned, therefore the SLS design is set as required.

2.8.3 Accidental Limit State

The structure must withstand when exposed to excessive structural damage as consequences of accident which affects the integrity of the structure, environment and personnel. The ALS could be, for example, collision of maintenance boat with the MCT, explosion of MCT due to excessive power production or electrical leak on generator and/or ground acceleration which causes seismic and tsunami.

2.8.4 Fatigue Limit State

The structure must withstand when exposed to cyclic loading that causes fatigue crack due to stress concentration and damage accumulation. This thesis will discuss in depth the fatigue design of MCT due to cyclic loading of wave and turbine at chapter 3.

3 FATIGUE DESIGN TERMINOLOGY

3.1 Introduction

Fatigue is a process of progressive localized permanent structural change in a material subjected to fluctuating stresses and strains at particular points that lead into cracks or complete fracture after a sufficient numbers of fluctuations. Marine current turbine (MCT) is exposed to fluctuating loads from wave and turbine. Therefore, the stress responses are varies in time which making MCT is prone to fatigue damage.

This chapter will expose the fatigue terminology starting with comparing the time series and frequency domain at section 3.2 and the principles of fatigue analysis afterwards. The selected fatigue spectral analysis is described in section 3.4 followed by stress concentration factor in section 3.5. Finally, section 3.6 will discuss the fatigue endurance of MCT support structure.

3.2 Time Domain vs. Frequency Domain

The time domain and frequency domain calculation methods offer two different analysis techniques for the same system. The main difference is that the time domain represents a specific of stochastic process and frequency domain covers all stochastically possible realisations.

The load calculation in frequency domain introduces a non-linearity through the drag term in the Morison equation. For offshore structures with pile configurations, it shows that the linear inertia term is more dominant compare to drag term. This applies for both maximum waves and smaller waves which induce fatigue loading at reference sites. As this system can be approached by linear term, the linear frequency domain can assess the fatigue damage calculation in an effective manner without losing accuracy as compared to time domain calculations. On the other hand, the time domain offers the exact value which fit in the excitation loading. It has precision loading as translated from environment condition present at reference site. However, in the oil and gas industry, this method is barely used due time consuming in the process of calculation. Therefore, the frequency domain fatigue analysis will be used and discussed in this thesis.

Table 3-1 provides the relation between time series and spectral parameters for waves which will be used in this thesis. The spectra formulation of JONSWAP and Pierson-Moskowitz can be found at section 2.4.2.

Table 3-1 : Time Series and Spectral Parameters for Waves

Description	Relation
Spectral moments ($n = 0, 1, 2, \dots$)	$m_n = \int_0^{\infty} f^n S(f) df$
Variance or mean square	$\sigma^2 = m_0$
Standard deviation or root mean square (RMS)	$\sigma = \sqrt{m_0}$
Significant wave height	$H_s \approx 4\sigma$
Mean zero crossing period	$T_z = \sqrt{\frac{m_0}{m_2}}$
Mean period of the spectrum	$T_m = \frac{m_0}{m_1}$
Mean crest period	$T_c = \sqrt{\frac{m_2}{m_4}}$
Maximum wave height	$H_{max} = 1.86 H_s$

3.3 Principles of Fatigue Analysis

3.3.1 Introduction

Fatigue in offshore structures is caused by the cumulative effect of all variable loads experienced by the structure during its life time. The variable loads from global and local loading are the main components for fatigue damage calculation. In addition, fatigue damage is highly localized type of failure affected by local details of structure connection. Therefore, the structure connection must be correctly represented in a fatigue analysis.

There are three main elements of fatigue damage analysis i.e.:

- Long term stress environment in each component
- Local hot spot stress calculation at each detail
- Fatigue endurance calculation of each detail.

Furthermore, the main principles of fatigue analysis due to associate loadings are outlined in this section which is taken from API RP 2A, Eurocodes and DnV RP C203.

3.3.2 Long-term Stress Environment

The long-term stress environment involves long-term wave climate, evaluation of wave loading on the structure, evaluation of structural internal loading and local hot spot stress accumulation analysis.

There are three commonly used methodologies in long-term stress environment analysis i.e. simplified, deterministic and spectral analysis which require different computational effort and have a different level of accuracy. The differences and applicability of each methodology are described here after.

3.3.2.1 Simplified Analysis

This method requires least computational effort. It uses the most simplified representation of the long-term wave environment and the associate loading. A single regular wave from long-term wave height statistics is used to estimate the long-term stress statistics. Thus, this method is appropriate for screening during the initial phase of the design.

3.3.2.2 Deterministic Analysis

This method has the similarity with previous method; the difference is a series of periodic waves with different heights and periods is used instead of a single regular wave to evaluate structural response. It counts non-linear wave loading but still not reflecting the true frequency content of the wave environment. Therefore, this method is appropriate for screening during initial design phase and may be used for final verification of structure in shallow and medium water depth where dynamic effects can be neglected.

3.3.2.3 Spectral Analysis

The spectral analysis is the best method to represent the random nature of the wave environment and its associate loading. Although linearization of wave loading and approximation of inundation effect is required, the spectral analysis counts the range of wave frequencies present in random seas and also suitable for dynamically responding structures. Therefore, this method is appropriate for final verification of fatigue design and will be used in this dissertation. Section 3.4 will discuss the spectral analysis in more detail.

3.3.3 Local Hot Spot Stress Calculation

The local hot spot stress is influenced by local details and its geometry and calculated from gross distributed load or nominal stress in the component.

Fatigue life of all details subjected to cyclic loading are required to be checked, however, special attention will be given to tubular joints since it mostly used in offshore structure design. The tubular joint configuration uses stress concentration factors (SCFs) to calculate the local hot spot stress from nominal member stress. Appropriate SCF formulation for tubular joints will be outlined in section 3.5.

3.3.4 Fatigue Endurance

The crack growth behaviour under cyclic loading for a particular material and detail defines the fatigue life of the structure. The fatigue endurance is translated from a given stress ranges to a number of cycles at particular location through S-N curve. Both stress range and number of cycles are in conjunction with long-term statistics of hot spot stresses and Miner's rule. The fatigue endurance which involves S-N curve and Miner's rule will be discussed in section 3.6.

3.3.5 Safety Philosophy

The main objective of fatigue analysis is to verify that the structure is safe due to associate fatigue loadings during its service life. The safety philosophy of fatigue design is to minimize the requirement of inspection and additional consideration should be given for inaccessible or difficult to inspect in-service area.

The following criteria may be applied for fatigue safety philosophy design:

- Easily accessible inspection should have a minimum calculated design fatigue life of twice of the intended service life.
- Inaccessible or difficult inspection should have a minimum calculated design fatigue life of four times the intended service life.

For the MCT support structure design, the details are considered as inaccessible or difficult to inspect therefore a minimum calculated design fatigue life of four times the intended service life is required.

3.3.6 Dynamic Analysis

Dynamic analysis is required if the natural periods of the structure are in the range of associate loadings which could lead to significant dynamic response.

For normal structure configuration in the oil and gas industry, dynamic response to wave can be ignored if the platform fundamental natural period is less than 3 seconds. And for mono-column type of structure, a lower wave period cut-off should be considered due to no wave cancelation effect at higher frequency.

3.4 Spectral Fatigue Analysis

3.4.1 Introduction

The spectral fatigue analysis is the most comprehensive analysis and the best way to represent the random nature of the wave environment. This method uses long-term

statistics of the wave tabulated in wave scatter diagram to represent the range of wave frequencies of reference site. These frequencies are explicitly accounted in the loading and structure response as well as the effect of hot spot stress transfer function for evaluating the response statistics for each random seastate. In addition, this method is ideal for dynamically responding structures.

3.4.2 Hot Spot Stress Transfer Function

The hot spot stress transfer functions are required for fatigue check in the structure. It defines the hot spot stress amplitude per unit wave amplitude over a range of wave frequencies at each wave direction.

The transfer function is determined by stepping a regular wave to the structure to calculate the cyclic loads on elements. This stepping regular wave height and frequency are selected carefully to achieve an appropriate transfer function which will be described in section 3.4.3 and 3.4.4 respectively. Structure analyses are then performed to calculate the hot spot stress range at location of interest. The result is divided by wave height to determine the transfer function which is equivalent to the hot spot stress amplitude per unit wave amplitude. This calculation is repeated for each frequency and direction at each point in the structure to establish a complete set of hot spot transfer functions.

Figure 3-1 shows the regular wave loading stepping to the structure and the structure response for particular frequency. For harmonic input load $F(t) = \hat{F} \cos(2\pi f \cdot t)$, the system response can be expressed analytically by equation (3-1).

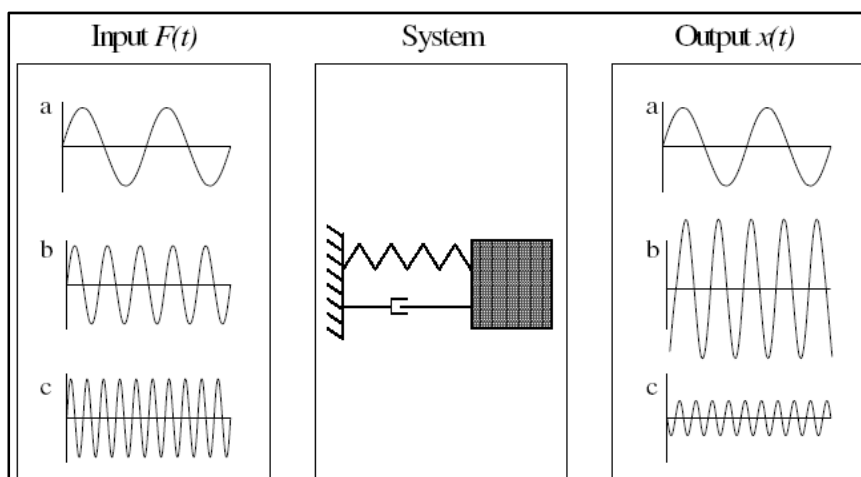


Figure 3-1 : Harmonic Sinusoidal Wave and Harmonic Structure Response Wave

$$x(t) = \hat{x} \cos(2\pi f \cdot t - \varphi)$$

$$\dot{x}(t) = -2\pi f \cdot \hat{x} \sin(2\pi f \cdot t - \varphi)$$

$$\ddot{x}(t) = -4\pi^2 f^2 \cdot \hat{x} \cos(2\pi f \cdot t - \varphi) \tag{3-1}$$

- Where
- $x(t)$ = body displacement [m]
 - $\dot{x}(t)$ = body velocity [m/s]
 - $\ddot{x}(t)$ = body acceleration [m/s²]
 - \hat{x} = displacement amplitude [m]
 - f = excitation frequency [Hz]
 - t = time [s]
 - φ = phase angle [rad]

By substituting equation (3-1) to (2-27), with replacing $u(t)$ by $x(t)$, the system can be re-written by equation (3-2). Once the solution has been found, the structure transfer function can be determined. Figure 3-2 shows the transfer function of the structure with body displacement amplitude per load excitation amplitude over frequency domain.

$$-m \cdot 4\pi^2 f^2 \cdot \hat{x} \cos(2\pi f \cdot t - \varphi) - c \cdot 2\pi f \cdot \hat{x} \sin(2\pi f \cdot t - \varphi) + k \cdot \hat{x} \cos(2\pi f \cdot t - \varphi) = \hat{F} \cos(2\pi f \cdot t) \tag{3-2}$$

- Where
- m = mass [kg]
 - c = damping coefficient [Ns/m]
 - k = spring constant [N/m]
 - $F(t)$ = harmonic excitation [N]
 - \hat{F} = load amplitude [N]

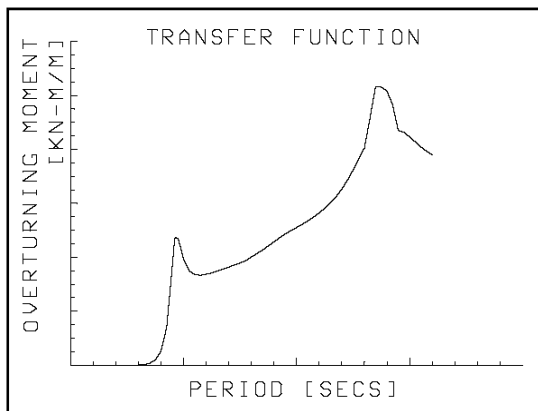


Figure 3-2 : Structure Transfer Function

As the response spectrum can be expressed by $S_x(f) = \frac{1}{2} \hat{x}^2(f) / \Delta f$, the transfer function can be determined by equation (3-3).

$$\begin{aligned}
 S_x(f) &= \lim_{\Delta f \rightarrow 0} \frac{1}{2} \frac{\hat{x}^2(f)}{\Delta f} = \lim_{\Delta f \rightarrow 0} \left[\frac{\hat{x}(f)}{\hat{F}(f)} \right]^2 \cdot \frac{1}{2} \frac{\hat{F}^2(f)}{\Delta f} = \left[\frac{\hat{x}(f)}{\hat{F}(f)} \right]^2 \cdot S_F(f) \\
 S_x(f) &= [TRF]^2 \cdot S_F(f) \\
 TRF &= \left[\frac{S_x(f)}{S_F(f)} \right]^{1/2} = \frac{\hat{x}(f)}{\hat{F}(f)}
 \end{aligned} \tag{3-3}$$

Where	$S_x(f)$	= structure response spectrum	[m ² s]
	$S_F(f)$	= excitation spectrum	[N ² s]
	TRF	= transfer function of structure	[m/N]

3.4.3 Wave Height Selection

The wave selection is aimed to limit the non-linearity introduced by drag component in the wave loading. This can be done by using a constant wave steepness which provides a simple relation between wave height and wave frequency. The wave steepness can be expressed in equation (3-4) with typical values in the range of 1:15 to 1:25.

$$\begin{aligned}
 H &= S \cdot L \\
 L &= \frac{gT^2}{2\pi} = 1.56 T^2
 \end{aligned} \tag{3-4}$$

Where	H	= wave height	[m]
	S	= wave steepness	[-]
	L	= wave length	[m]
	g	= gravity acceleration ($g = 9.81$)	[m/s ²]
	T	= wave period	[m]

The use of constant wave steepness will introduce unrealistic large wave height at small frequencies. Therefore, limitation has been given with using minimum wave height of 0.3m (1 foot) and maximum wave height equal to the design wave height.

3.4.4 Wave Frequency Selection

The wave frequency selection is aimed to set a fine wave response over relevant frequency range. The followings describe the basis for frequency selection based on structure and environment characteristics.

- Minimum and Maximum Frequencies
 - The minimum and maximum frequency should cover the significant energy of the seastate.

- Cancellation and Addition Frequencies
 Wave frequency in the area of peaks and troughs should be included to get a fine shape of wave response.
- Intermediate Frequencies
 Sufficient intermediate frequencies should be included to ensure a complete definition of the transfer function features.
- Natural Frequencies
 The natural frequency should be included in order to define the peak of dynamic response. Three closely spaced additional frequencies on each side of natural frequency should also be included with maximum space is defined by critical damping of the structure.

Figure 3-3 shows the typical base shear wave load transfer function over frequency grid. The transfer function has to be checked to ensure the shape of peaks and valleys are clearly defined.

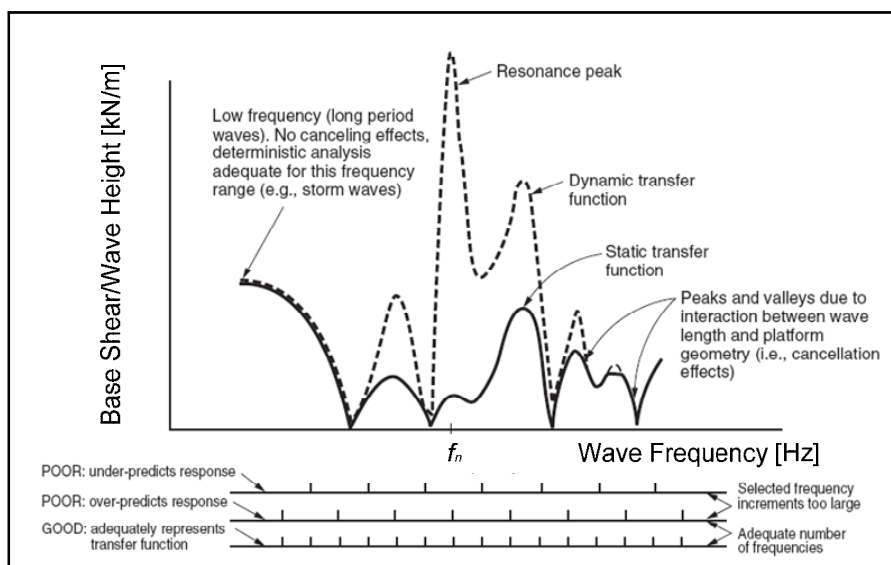


Figure 3-3 : Selection of Frequencies for Detailed Analyses (API RP 2A)

3.4.5 Wave Response

Frequency domain wave response analysis offers an efficient computational calculation for evaluating dynamic response of a linear problem with modal analysis.

For global structure response, modal analysis gives a reliable method. However, for local responses like fatigue analysis, the modal techniques are usually unreliable. One solution can be used by using a large number of modes but it contains numerical inaccuracies associated with high frequency modes. To overcome these problems, mode accelerations

method is introduced which superimposes the dynamic responses due to limited number of modes into a full static solution. This method can represent the significant dynamic response with reliable accuracy and computational efficiency by including a sufficient number of modes.

The SACS wave response module has capability to use equivalent static load to represent the loads on structure due to fluid motion including the relative motion between structure and fluid. The equivalent static load consists of inertia and hydrodynamic loadings which come from modal acceleration and the fluid-structure motion respectively. As the high frequency modes has static response, the dynamic amplification will significantly occur at low frequency overall structural modes. Thus, the significant inertia loads can be found in this range. The equivalent static load eliminates large number of modes by adding inertia loading that has significant dynamic amplification to the actual hydrodynamic loading. In the oil and gas industry, it is recommended to use this technique if not specified in the design criteria.

3.4.6 Linearization of Non-linear Wave Loads

The load calculation is based on water particle velocity and acceleration as discussed in section 2.4. The particle motion can be approached by several theories; however, the Airy wave linear theory is the most accurate theory to model this linearity. According to Airy theory, the particle velocities and accelerations are linearly dependent on the wave amplitude.

The non-linear wave load is only introduced by drag term of Morison equation as seen on equation (3-5) or (2-10) which shows the square of the velocity in the drag term.

$$q_{hydro} = f_i + f_d = \frac{\pi}{4} \rho_w C_M D^2 \cdot \dot{u} + \frac{1}{2} \rho_w C_D D \cdot |u|u \quad (3-5)$$

The total hydrodynamic load and overturning moment on a single pile with uniform diameter can be determined by integrating f_i and f_d from sea bed to free water surface elevation as expressed by equation (3-6).

$$F(t) = \int_{-d}^{\zeta} \{f_i(z, t) + f_d(z, t)\} dz$$

$$M(t) = \int_{-d}^{\zeta} \{f_i(z, t) + f_d(z, t)\} \cdot (d + z) dz \quad (3-6)$$

Where $F(t)$ = total hydrodynamic load [N]

$M(t)$	=	overturning moment	[Nm]
f_i	=	hydrodynamic inertia load per unit length	[N/m]
f_d	=	hydrodynamic drag load per unit length	[N/m]
ζ	=	water surface	[m]
d	=	mean water depth	[m]

Simplification of equation (3-6) can be used by setting the integration from seabed to still water level ($z = 0$). This method discard the drag force acting on pile during the passage of wave crest but does not affect the inertia load as the maximum load occurs when the wave surface at zero crossing. Although this condition can be significant at drag dominated term, it has shown that for this particular application, this simplification is still valid. As the pile diameter is much smaller than the excitation wave, the governed wave loading is mainly due to inertia. For less extreme wave condition, fatigue waves, the inertia loading dominates the total hydrodynamic loading. Therefore the wave induced fatigue will be influenced by linear inertia wave loading. The magnitude of drag and inertia load and moment can be expressed by equation (3-7).

$$\begin{aligned}
 F_i &= \frac{\pi}{4} \rho_w g C_M D^2 \zeta_a \cdot \tanh(kd) \\
 F_d &= \frac{1}{2} \rho_w g C_D D \zeta_a^2 \cdot \left[\frac{1}{2} + \frac{kd}{\sinh 2(kd)} \right] \\
 M_i &= \frac{\pi}{4} \rho_w g C_M D^2 \zeta_a \cdot d \left[\tanh(kd) + \frac{1}{kd} \left(\frac{1}{\cosh(kd)} - 1 \right) \right] \\
 M_d &= \frac{1}{2} \rho_w g C_D D \zeta_a^2 \cdot \left[\frac{d}{2} + \frac{2(kd)^2 + 1 - \cosh 2(kd)}{4k \sinh 2(kd)} \right]
 \end{aligned}
 \tag{3-7}$$

Where	F_i	=	inertia load	[N]
	F_d	=	drag load	[N]
	M_i	=	inertia moment	[Nm]
	M_d	=	drag moment	[Nm]
	ρ_w	=	mass water density	[kg/m ³]
	g	=	acceleration of gravity	[m/s ²]
	k	=	wave number	[rad/m]
	C_M	=	inertia coefficient	[-]
	C_D	=	drag coefficient	[-]
	D	=	diameter of pile	[m]
	ζ_a	=	wave amplitude	[m]

3.4.7 Natural Frequency

The natural frequency of the MCT support structure depends on design configuration and mass at the top of tower. The theoretical frequency should be reviewed and selected carefully as expressed in equation (2-29) and described in Figure 2-21. The position of natural frequency defines the level of dynamic response. Resonance would occur if the natural frequency is in the vicinity of excitation frequency of the wave or turbine and might lead to structure failure. If the natural frequency falls in a valley of the base shear wave load transfer function, it should be shifted by 5 to 10% to a more conservative location. This can be done by adjusting the mass or stiffness parameters of the MCT support structure. The choice of modification depends on the support structure type, mass and soil conditions. Since the top mass is relatively fixed by turbine manufacturer, the adjustment has to be made in the stiffness of MCT support structure by changing the diameter of tower and pile. However, the foundation stiffness modification may sensitive to fatigue analysis.

3.4.8 Short-term Hot Spot Stress Statistics

After calculating the hot spot stress transfer function for all locations in the structure, the short-term statistics of hot spot stress are calculated using standard spectral as described in section 2.4.2. The short-term statistics indicates the numbers that the hotspot stress range exceeds a certain value at one occurrence for a particular approach direction.

The hot spot stress transfer function for a particular location and wave direction are tailored with the spectrum to calculate the hot spot stress response spectrum for each seastate. The Root Mean Square (RMS) value and mean period of the hot spot stress response are determined by integration function of the spectrum and its higher moments. These components are to be used for probability distribution function of peak value to achieve the short term statistics of the hot spot stress range.

For narrow banded process, the Rayleigh probability distribution function is normally used, while Rice probability distribution function is valid for Gaussian random process of any width. In practice, Rayleigh probability distribution is appropriate for relatively similar waves and Rice can be used for varies wave data.

Rayleigh Probability Distribution Function

The Rayleigh distribution is based on the zeroth moment of the spectrum as expressed by equation (3-8).

$$P_{Rayleigh}(s_i) = 1 - e^{-\frac{s_i^2}{2m_0}}$$

$$P_{Rayleigh}(S_i) = 1 - e^{-\frac{S_i^2}{8m_0}}$$
(3-8)

Where

s_i	= stress amplitude	[N/m ²]
S_i	= stress range ($S_i = 2s_i$)	[N/m ²]
m_0	= zeroth moment of spectrum	[-]

The number of stress ranges per stress range class can be expressed by equation (3-9).

$$n_i(S_i) = \frac{T_d}{T_z} [P_{Rayleigh}(S_{i+1}) - P_{Rayleigh}(S_i)]$$

$$= T_d \sqrt{\frac{m_2}{m_0}} \left[e^{-\frac{S_i^2}{8m_0}} - e^{-\frac{S_{i+1}^2}{8m_0}} \right]$$
(3-9)

Where

n_i	= number of cycles present at stress range i	[-]
T_d	= duration of the state	[s]
T_z	= average period between stress range	[s]

Rice Probability Distribution Function

The Rice distribution is based on the zeroth, second and fourth order moment of the spectrum as expressed by equation (3-10).

$$P_{Rice}\left(\frac{1}{2}S_i\right) = P_{Rice}(s_i) = P_N\left(\frac{s_i}{\varepsilon\sqrt{m_0}}\right) - \sqrt{1-\varepsilon^2} \cdot e^{-\frac{s_i^2}{2m_0}} \cdot P_N\left(\frac{s_i\sqrt{1-\varepsilon^2}}{\varepsilon\sqrt{m_0}}\right)$$

$$P_N = \frac{1}{\sqrt{2\pi}} \int_{-\infty}^x e^{-\frac{1}{2}t^2} dt$$

$$\varepsilon = \sqrt{1 - \left(\frac{T_c}{T_z}\right)^2} = \sqrt{1 - \frac{m_2^2}{m_0 m_4}}$$
(3-10)

Where

P_N	= cumulative prob. of standard normal distribution	[-]
ε	= spectral width parameter	[-]
m_2	= second moment of spectrum	[-]
m_4	= fourth moment of spectrum	[-]

The number of stress ranges per stress range class can be expressed in equation (3-11).

$$\begin{aligned}
 n_i(S_i) &= \frac{T_d}{T_c} [P_{Rice}(S_{i+1}) - P_{Rice}(S_i)] \\
 &= T_d \sqrt{\frac{m_4}{m_2}} [P_{Rice}(S_{i+1}) - P_{Rice}(S_i)]
 \end{aligned}
 \tag{3-11}$$

Where n_i = number of cycles present at stress range i [-]
 T_c = average crest period [s]

3.4.9 Long-term Hot Spot Stress Statistics

The long-term hot spot stress statistics is basically the accumulation of short-term hot spot stress statistics of all seastates and directions. This summation is done after applying the probability of occurrence of the seastate and the wave direction. This cumulative distribution is to be used as an input to the fatigue damage calculation and will be described in section 3.6.

3.4.10 Overview Frequency Domain Spectral Fatigue Analysis

To summarize, Figure 3-4 shows the sequence of transfer function calculation and the structure response due to wave. This method can be applied to all wave spectra tabulated in scatter diagram for all directions which making the calculation efficient and fast.

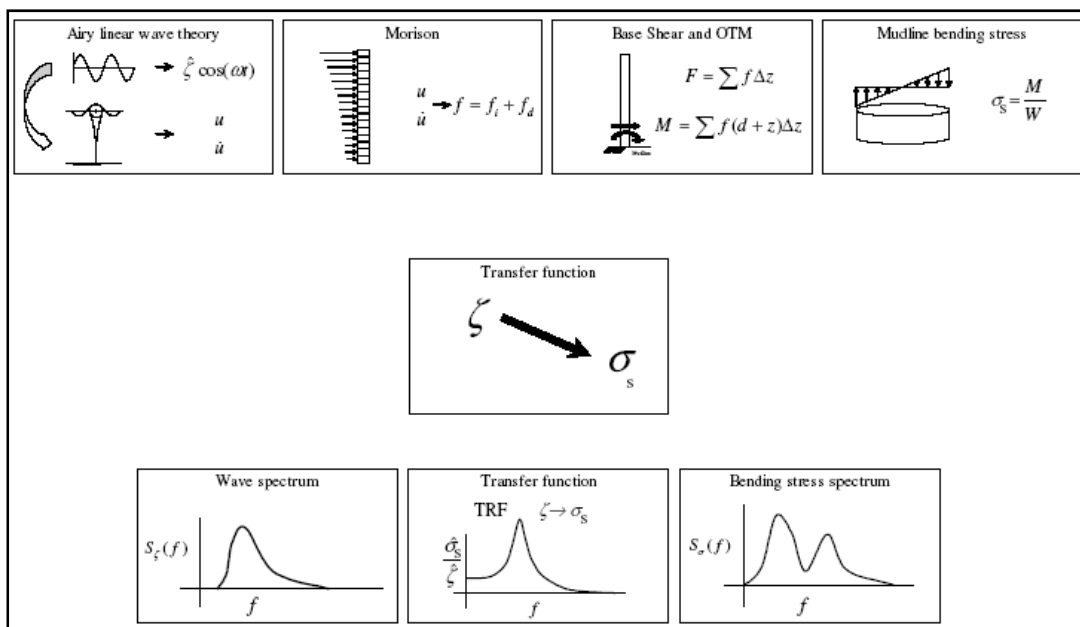


Figure 3-4 : Overview Frequency Domain Spectral Fatigue Analysis [38]

3.5 Stress Concentration Factor

The structural analysis explained at previous sections provides nominal axial, in-plane and out-plane bending stresses at all points of interest. The fatigue check of particular detail can

be performed by adding the local hot spot stress with stress concentration factor (SCF) which accounts the effect of geometry of the detail on the local stress distribution. Different SCFs may apply on the nominal stress components depend on the geometry of the detail. The combination of SCFs and nominal stress components produces the peak hot spot stress. In addition, the SCFs should be compatible with nominal stresses and S-N curve.

The stress concentration factors for commonly occurring details are available in standards or codes. For simple geometry, it can be calculated directly. For more complex connection, parametric formulae are introduced which derived from model tests or finite element analyses. In case of unusual connection that does not apply to any codes or standards, detailed finite element analysis is required to determine the SCF.

The commonly used SCF's equation is provided by Efthymiou. It consists parametric equations for T, Y, K, KT and X-joint configurations under axial load, in-plane bending and out-plane bending. The SCF should be applied to the chord or brace side of the tubular intersection weld.

The standards or codes of SCF can be found in API RP 2A and DnV RP C203 for other details like tubular thickness transition.

3.6 Fatigue Endurance

3.6.1 Introduction

From spectral fatigue analysis, the long-term hot spot stress range statistics has been produced in form of number of cycles. These statistics are to be used in fatigue endurance calculation using an appropriate S-N curve for each connection detail in conjunction with Miner's rule for linear accumulation of the fatigue damage. For welded structures, the most sensitive to fatigue failure are normally associated with the weld itself and the details of the welds in respect of geometry and welding particulars.

3.6.2 S-N Curve

The S-N curve provides the allowable numbers of cycles failed due to fatigue at particular stress range. The commonly used standards of S-N curves can be found in API, Eurocodes and DnV. For example, API X and X-prime for simple tubular connections can be found in API RP 2A. However, the most comprehensive set of S-N curves can be found in DnV RP C203 which covers a broad range of connection details.

The selection of S-N curves is based on the direction of applied stresses, the fabrication method and the inspection method.

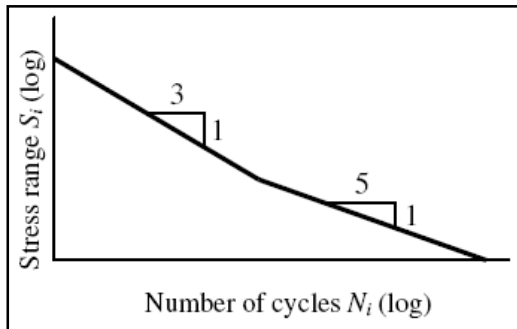


Figure 3-5 : Typical S-N Curve for Structural Detail

Figure 3-5 shows the typical S-N curve for steel material with slope of 3 at lower cycles and slope of 5 at higher cycles. The stress range and number of cycles axes are in log-log domain.

3.6.3 Miner's Rule

The Miner's rule provides the cumulative fatigue damage calculation for linear approach. It enables the constant amplitude design of S-N curves to be applied in the structure exposed to variable amplitude loadings. The Miner's rule has the reliability to predict the actual fatigue lives due to variable amplitude loading, particularly for welded connection. The fatigue damage ratio based on Miner's rule is expressed by equation (3-12).

$$D_r = \sum_i \frac{n_i}{N_i} \quad (3-12)$$

Where D_r = cumulative fatigue damage ratio [-]
 n_i = number of cycles present at given stress range S_i [-]
 N_i = allowable number of cycles at given stress range S_i [-]
 S_i = stress range at i [kN/m²]

The Miner's rule states that the detail is considered safe due to fatigue if $D_r < 1$.

The design fatigue life is determined by the inverse of the cumulative fatigue damage ratio in yearly basis.

$$\text{Design Fatigue Life} = \frac{1}{D_r} \quad (3-13)$$

4 METHODOLOGY

4.1 Introduction

This methodology can be used as general fatigue design of marine current turbine (MCT) approached by frequency domain analysis. Structure Analysis Computer System (SACS) ver.5.2 computer programme is used to calculate the fatigue performance of the structure. Engineering Dynamic, Inc. (EDI) has developed the SACS system of software for offshore structure engineering applications. SACS consists of several modular structural analysis programmes which are interface to each other. Further detail of the software can be read on SACS manual attached to the software.

The fatigue analysis on MCT has not been developed by SACS. Therefore, in this thesis, the fatigue analysis and calculation are based on experience and expertise engineering judgement. The methodology is also applied to a range of representative cases which will be discussed in this chapter.

The overview of MCT design methodology is described in section 4.2 followed by analysis set-up for wave induce fatigue and turbine induce fatigue in section 4.3 and 4.4 respectively. Section 4.5 covers the MCT support structure, section 4.6 explores the environment data present in the reference site and finally, section 4.7 describes the computer model used in this thesis.

4.2 Overview of Methodology

The methodology for calculating fatigue performance of structure is divided into two modules of excitation sources. Current flow moves the blades for electricity generation which causes vibration in the support structure. Excitation from stochastic process of the wave is the other source in fatigue analysis design. By these specific sources, vibration module and wave response module in SACS can be used to predict the analytical fatigue performance of the support structure.

First, the turbine is modelled on a rigid support structure with a constant rotational speed. Transfer function of this model can be determined by extraction of structure response over excitation input. Then, wave excitation is modelled including hydrodynamic damping as the effect of operating turbine. Stress variation due to wave and turbine generated current are now can be calculated. By assuming the wave and current induced stresses are independent

to each other, the final stress response can be determined by quadratic superposition. Figure 4-1 shows the overview of fatigue performance calculation due to wave and current.

Fatigue performance of MCT is not only affected by operating and idling condition but also by start-up, stoppages and pile driving activities. These cases can be analyzed independently and added to the total fatigue damage. Since the operating and idling cases are the most governing conditions for fatigue, therefore these cases are to be considered in this thesis.

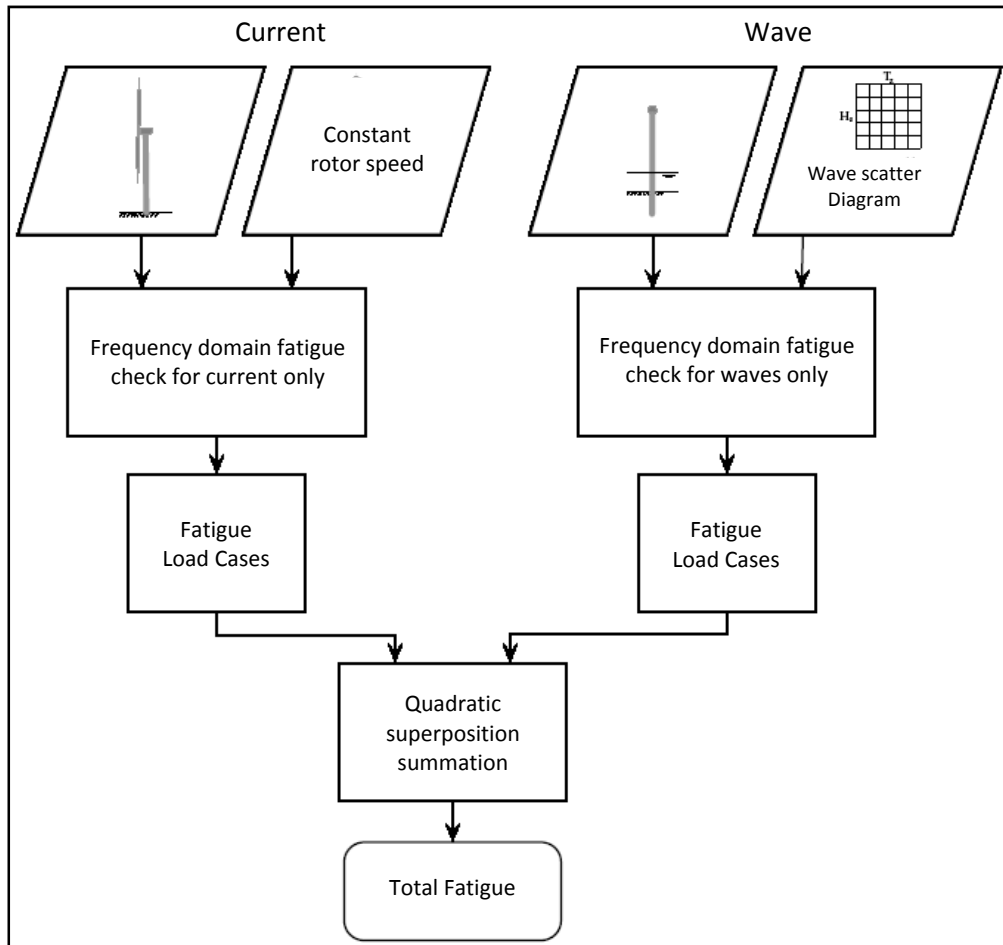


Figure 4-1 : Overview of Fatigue Analysis Methodology for Current and Wave

4.3 Analysis Set-up Wave Induce Fatigue

The followings are the general steps of fatigue analyses due to wave excitation:

- Detailed computer model represents the structure mass, damping, stiffness and hydrodynamic properties.
- Natural frequencies and modal analysis.
- Wave response analysis for each direction to evaluate the nominal stress range.
- Stress Concentration Factors (SCF's) combined with nominal stress range to achieve peak hot spot stresses for each chord-brace interface.

- Fatigue damage calculation based on appropriate S-N curve in conjunction with peak hot spot stress and number of wave occurrence.
- Cumulative fatigue damage evaluation using Miner's rule to determine the corresponding service life of the structure.
- This service life is compared to the design life. If the service life is more than the design life, joint is considered acceptable.

Table 4-1 shows the detailed procedure flow chart for SACS computer program.

Table 4-1 : Spectral Fatigue Analysis Procedure

No	Input	Program Execution	Output
1	PILE-SOIL INTERACTION ANALYSIS		Generate Foundation Linearization
	Structural Data	<i>Static with Soil Pile Interaction</i>	Foundation Linearization File
Soil Data	Output Listing		
2	FREE VIBRATION ANALYSIS		Generate Natural Period
	Structural Data	<i>Extract Mode Shapes</i>	Mass File
	Dynamic Data		Modes File
Foundation Linearization File	Output Listing		
4	WAVE RESPONSE ANALYSIS		Generate Dynamic Transfer Function
	Wave Data	<i>Wave Response</i>	Common Solution File
	Structural Data		Output Listing
	Mass File		
	Modes File		
Foundation Linearization File			
4	FATIGUE DAMAGE ANALYSIS		Generate Fatigue Life
	Fatigue Data	<i>Fatigue Damage</i>	Output Listing
Common Solution File			

Note: coloured boxes indicate analysis output to be used as input in the next steps.

STEP – 1: Pile Soil Interaction (PSI) Analysis.

As the dynamic analysis is using linear theory, the non-linear pile-soil-interaction must be represented in a linear equivalent system. PSI analysis is used to generate the equivalent foundation stiffness matrix or SuperElement file to represent the foundation for dynamic

analysis. Since fixed linear foundation is to be applied in analysis, thus this step can be neglected.

STEP – 2: Free Vibration Analysis

Free vibration analysis is performed to determine the dynamic characteristic of the structure. This includes natural periods, mode shapes and modal internal load and stress vectors. This module generates the structural mass for all modelled elements and associate loadings. In addition, the added mass of entrapped fluid in members is also considered.

STEP – 3: Wave Response

The wave response module is used to compute the dynamic response of the structure subjected to wave action. The wave response program interacts with the dynamic analysis program to produce modal response in order to calculate the internal load members. This internal load on each member is described as Common Solution File (CSF).

From the wave data, the numbers of wave heights with corresponding periods are used to define the relationship between wave height and stress range. The stress range for each wave and the number of occurrence is then used to determine fatigue damage.

STEP – 4: Fatigue Damage Analysis

Fatigue is a post-processing program in SACS to evaluate the structure performance with respect to fatigue failure. It uses the results of dynamic and wave response analysis to evaluate the stresses for tubular cross sections around the welded connections. The stresses are then multiplied by stress concentration factors and stress ranges are evaluated.

The resulting stress ranges are then used to find the damage rates at each of the eight points of joint tubular cross section by calculating the ratio of the number of occurrences of this stress range to that which would produce failure as determined from S-N curve.

4.4 Analysis Set-up Turbine Induce Fatigue

The fatigue damage due to turbine loading has not been developed in SASC yet. Therefore, approximation will be made by adopting the above steps and used Engine Vibration Analysis instead of Wave Response Analysis to evaluate the nominal stress range of the turbine. The total service life of the structure is evaluated by merging the cumulative fatigue damage from each analysis.

4.5 Description of the MCT Support Structure

The fatigue design of marine current turbine will be modelled by three different types of support structure (monopile, tripod and GBS) at three different water depths (20m, 30m, and 40m) as shown in Figure 4-2 and Figure 4-3 to accommodate the characteristics of site condition.

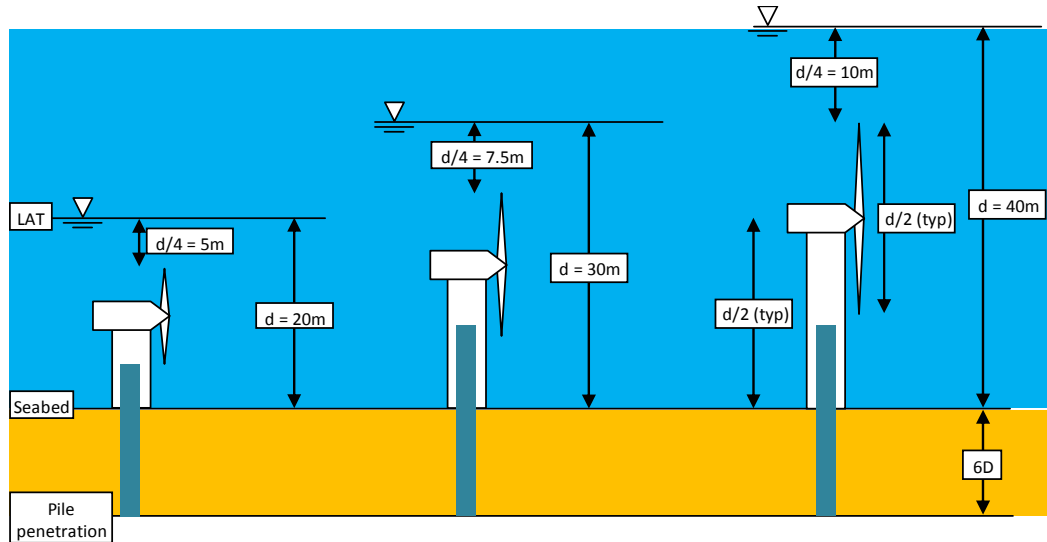


Figure 4-2 : Water Depth Configuration for Monopile MCT Support Structure

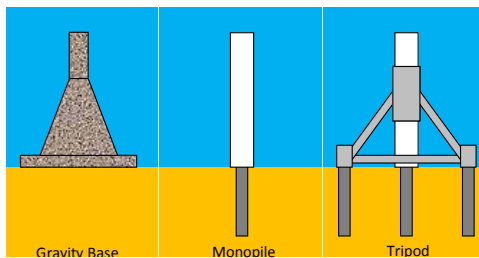


Figure 4-3 : MCT Support Structure Configuration

4.6 Environment Data

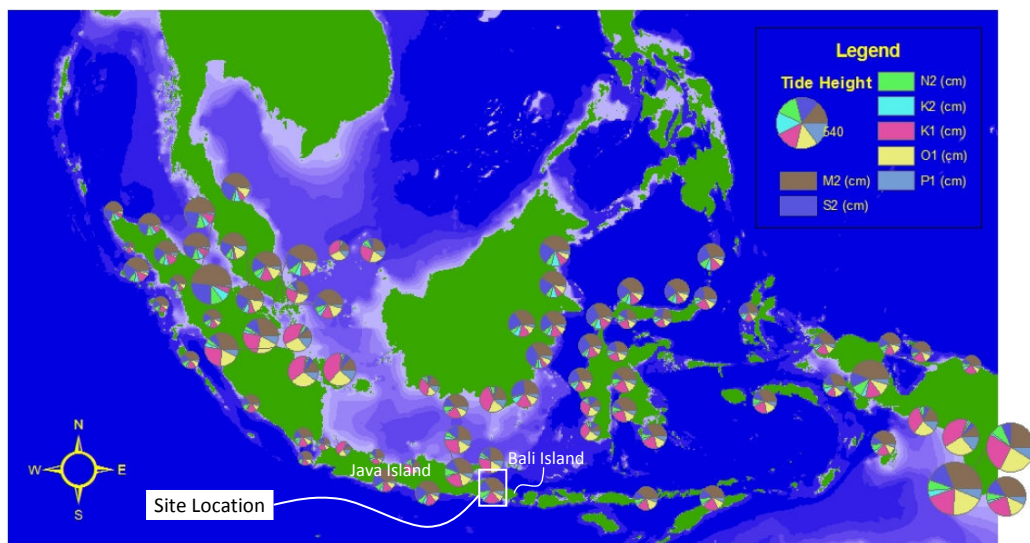


Figure 4-4 : Tidal Constituents in Indonesia [22]

Figure 4-4 shows the tidal constituent present in Indonesia water. The tidal characteristics are mainly mixed but semi-diurnal dominated. The reference site location between Java and Bali islands is selected for this thesis as marked with white box in Figure 4-4. Bali Island is well known as paradise of the tropical and invites most of tourists in Indonesia. Therefore, the island requires more energy to fulfil its demand.

The detail data of reference location is obtained from Pagerungan Station [29] which consists of current, wave and marine growth data.

4.6.1 Current Data

Currents are varies widely overtime in both velocity and direction. The presence of current with conjunction with wave will affect the total drag loading and will change the magnitude of the cyclic loading. Sensitivity calculation has shown that the effect of current is generally small. In oil and gas industry, therefore, current are normally ignored for fatigue analysis. However for MCT fatigue design, current presence will be included in calculation. Table 4-2 shows the current speed over percentage of water depth elevations.

Table 4-2 : Current Data over Depth [29]

Elevation % of water depth	Current Velocity
0	0.55 m/s
10	0.53 m/s
20	0.52 m/s
30	0.50 m/s
40	0.48 m/s
50	0.46 m/s
60	0.44 m/s
70	0.41 m/s
80	0.38 m/s
90	0.35 m/s
100	0.32 m/s

4.6.2 Wave Data

Waves are the dominant source of fatigue loading on offshore substructures. Long-term wave environment is required for fatigue analysis to enable the cumulative effect of all wave conditions occurring throughout structure life time. Wave scatter diagram, which is the probability of occurrence of seastate defined by significant wave height (H_s) and associated zero crossing period (T_z), is the most suitable representing wave condition for fatigue analysis. The data may be obtained by measurements, hind casting or combination of both.

Table 4-3 and Figure 4-5 show the directional wave scatter diagram and the probability of occurrence of wave period in Pagerungan station. It indicates individual probabilities for number of mean approach directions.

Table 4-3 : Percentage Wave Occurrence at Pagerungan station [29]

Direction	Significant wave height groups (m)						Total
	0.1 – 0.5	0.5 – 1.0	1.0 – 1.50	1.50 – 2.00	2.0 – 2.5	> 2.5	
N	0.48	0.92	2.48	0.18	0.75	0.10	4.90
NE	0.56	0.49	0.99	0.03	0.11	0.01	2.19
E	0.52	1.31	4.63	1.05	3.42	2.38	13.32
SE	0.67	1.83	7.64	2.59	5.43	3.18	21.34
S	0.52	0.99	2.29	0.23	0.41	0.03	4.46
SW	0.56	0.63	1.53	0.11	0.10	0.00	2.93
W	0.70	1.68	5.78	1.41	3.37	0.85	13.78
NW	0.51	1.83	10.32	2.19	11.57	2.60	29.02
Total	4.52	9.69	35.64	7.79	25.16	9.14	100

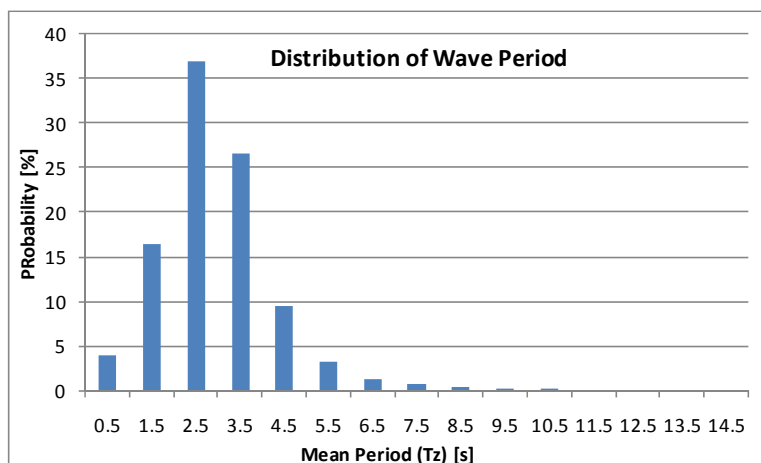


Figure 4-5 : Distribution of wave period for fatigue analysis at Pagerungan station [29]

4.6.3 Water Level

The water level for fatigue analysis should use the average water level during the life time of structure. In this case the water level is assumed at 20m, 30m and 40m above seabed to accommodate the site characteristics. Subsidence is not considered in this thesis; therefore, the water level is set to constant as stated previously.

4.6.4 Marine Growth

The presence of marine growth attached to the structure increases the total diameter exposed by water particles, consequentially the acting force is increasing. Marine growth is normally pronounced during the first few years after structure installation or establishment. For new design in Indonesian water, specifically at place of interest, the marine growth is

expected in value of 5cm (to the radius) between mean sea level to seabed with density of 1233 kg/m^3 .

4.7 Computer Model

4.7.1 Preliminary Design

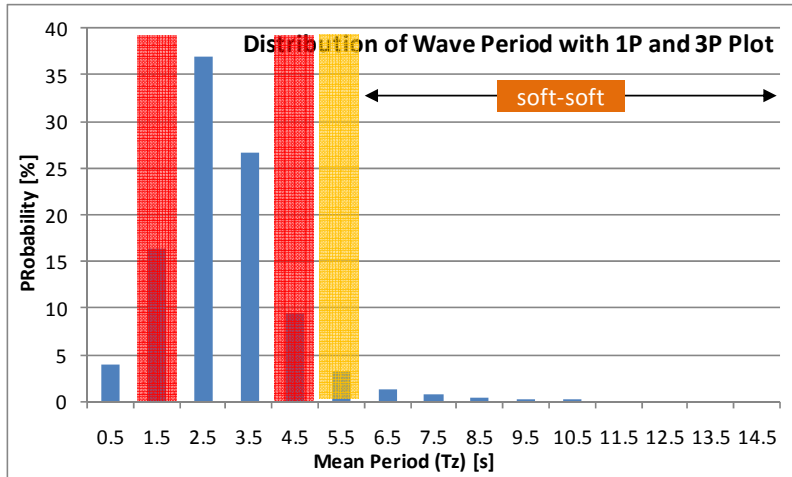


Figure 4-6 : Distribution of wave period for fatigue analysis with 1p and 3P Plot

Figure 4-6 shows the distribution of wave period with 1P and 3P plot as well as soft-soft range for support structure design natural period (inverse of natural frequency). As the wave probability distribution in reference site has short periods (blue thick bars) and the selected turbine constant speed of 10.5 RPM (red light bars) has excitation period of 5.7s and 1.9s for 1P and 3P respectively, it results that the soft-soft area is at $T_n \geq 6s$. This leads to a slender support structure configuration which requires special configuration.

By using equation (2-30) with a constant wall thickness (t_w) of 25mm and assumed top mass of $1 \times 10^4 \text{ kg}$, the relation between MCT natural period (T_n), water depth (L) and preliminary support structure diameter (D_{av}) can be determined as shown in Table 4-4. The natural period of the MCT is in the range of 6s-6.6s with less than 5% of resonance due to wave excitation occurs during its life time. However, the selection of natural period of MCT has to be in accordance with the wave extreme condition to avoid excessive deflection due to ultimate limit state design.

Table 4-4 : MCT Natural Period Selection

D_{av} [m]	t_w [m]	L [m]	f_n [Hz]	T_n [s]
0.250	0.025	20	0.17	6.02
0.375	0.025	30	0.16	6.26
0.500	0.025	40	0.15	6.59

4.7.2 Pile-Soil-Interaction Analysis

Clamped foundation model with fixity depth of 6D is considered in this thesis as described in section 2.7. Therefore, the foundation model for MCT support structure is in linear form in conjunction with the structure model.

4.7.3 Free Vibration Analysis

Specific inputs are required for free vibration analysis as described here after:

- Consistent Mass Option is chosen since it gives better estimated of calculated added mass.
- The linear foundation of 6D is used for carrying out the free vibration analysis.
- Retained degrees of freedom are specified on all main structural joints so as to obtain all the modes having higher mass participation factors.
- The pile is kept flooded for entrapped water mass in the natural frequency calculation.
- A total of 3 modes have been extracted to participate in spectral analysis.
- Added mass coefficient specified is equal to 1.0.
- The weight density of all members has been increased by 10% to account for miscellaneous weight contingency.

4.7.4 Fatigue Wave Climate

- Total number of wave used in fatigue analysis is 18519217 based on report “Final report of Metocean Design Criteria for General Kangean Block Area” by PT LAPI ITB, 29 August 2005. [29].
- Airy theory has been used to evaluate the hydrodynamic loading due to fatigue waves.
- A total of 12 wave directions is chosen to carry out fatigue analysis

4.7.5 Wave Response Analysis

By initiating the “Wave Response” module of SACS the wave response analysis is performed. The member hydrodynamic loads and member inertia loads due to the structural acceleration are computed simultaneously at every wave step position by using the model analysis method. A total of 3 modes computed from free vibration analysis has been used for obtaining the member inertial loads.

C_D and C_M are adopted from API RP 2A are specified below:

- For fouled members $C_D = 0.8$ and $C_M = 2.00$
- For clean members $C_D = 0.5$ and $C_M = 2.00$

To account for anodes and other non-modelled members, the increase in drag and inertia coefficient must be assessed, generally taken as 5% or as specified in the design criteria.

4.7.6 Fatigue Analysis

After obtaining the member end nominal stress, the fatigue analysis module of SACS is activated to carry out Joint fatigue analysis.

The following are the important data considered for Fatigue Analysis.

- S-N curves of DNV curve D, F, F3 and API-X Prime Curve for Estimation of Joint Fatigue Lives.
- Joint SCF has been computed by using formula as suggested by Efthymiou and is load path dependent. Joint SCF obtained by using this option are observed to be on conservative side.
- The Design Fatigue Life of joint is set to 20 years as a standard life design taken from offshore wind turbine.
- Life safety factor is set to 4.0 (see section 3.3.5).

5 ANALYSIS RESULT

5.1 Introduction

The minimum fatigue life of 80 years (20 years service life with factor of safety 4.0) is required as design basis in this thesis. Hence, this chapter will outline the analysis result of fatigue design of Marine Current Turbine support structure accordingly.

The fatigue design on monopile support structure is described in section 5.2 followed by gravity based support structure at section 5.3. Finally, the tripod type support structure is discussed in section 5.4.

5.2 Mono-pile Structure

The service life of monopile MCT support structure has been analyzed using three different detail connections based on DNV Curve F, F3 and D with constant wall thickness of 25mm. Figure 5-1 shows that the DNV curve D has the longest service life compare to curve F and F3. It also expresses that DNV curve D offers service life above required of 80 years (black thick horizontal line) in range of 4s and 8s of natural period (T_n) . Therefore, this type of details can be used at any point in that range. For DNV curve F and F3, natural period has to be selected carefully in order to fulfil the required service life of 80 years. Based on the analysis, natural period of 5.3s and 4.7s are the maximum recommended limit for DNV curve F and F3 respectively in order to fulfil required service life. Table 5-1 tabulates in detail the relationship between service life, natural period and monopile properties using a constant wall thickness at 40m water depth. For monopile configuration unless note otherwise, D , t_w and f_n represent the pile diameter, pile wall thickness and natural frequency of the support structure.

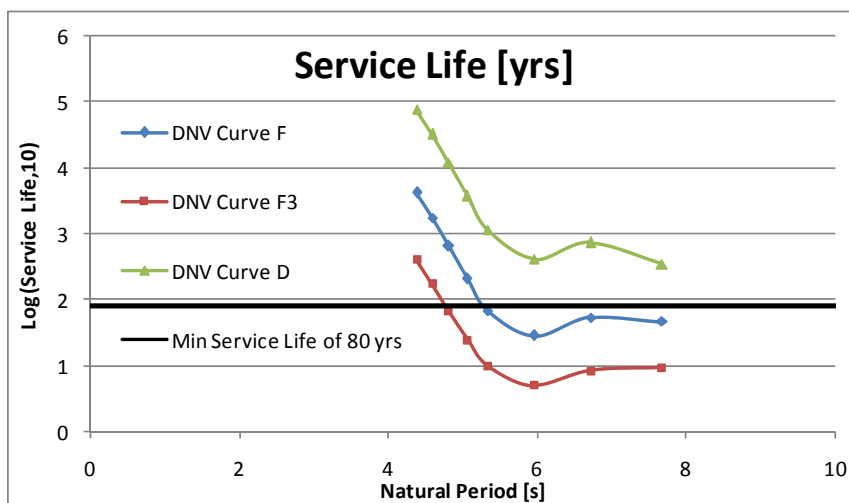


Figure 5-1 : Service Life of Monopile with Constant t_w of 25mm at 40m Water Depth

Table 5-1 : Service Life of Monopile with Constant t_w of 25mm at 40m Water Depth

No	D	T_n	f_n	Service Life		
				DNV curve F	DNV curve F3	DNV curve D
	[cm]	[s]	[Hz]	[yrs]		
1	40.00	4.386	0.228	4201	400	76395
2	38.75	4.592	0.218	1787	173	32563
3	37.50	4.817	0.208	651	67	11857
4	36.25	5.063	0.198	208	25	3728
5	35.00	5.332	0.188	69	10	1157
6	32.50	5.956	0.168	29	5	415
7	30.00	6.723	0.149	54	9	734
8	27.50	7.683	0.130	47	9	353

It is interesting to find out the effect of reduced wall thickness instead of diameter since it gives more beneficial such as total mass and strength properties. The red lines in Figure 5-2 represent the effect of wall thickness reduction at constant diameter of 400mm and it shows that wall thickness is sensitive to fatigue failure. For the same natural period, constant diameter has less service life compared to constant wall thickness at all curves of DNV. The DNV curve D now has limitation up to 5.5s of natural period (assumed linear relation). For curve F and F3, natural period reduces to 5s and 4.6s respectively. The reduction of service life is caused by reduction of cross section area of the monopile. When the cross section area is reduced, the welding area becomes smaller and narrower therefore the connection strength and service life are reduced. Table 5-2 tabulates in detail the relationship between service life, natural period and monopile properties using constant diameter at 40m water depth. Pile wall thickness is represented by t at centimetres unit.

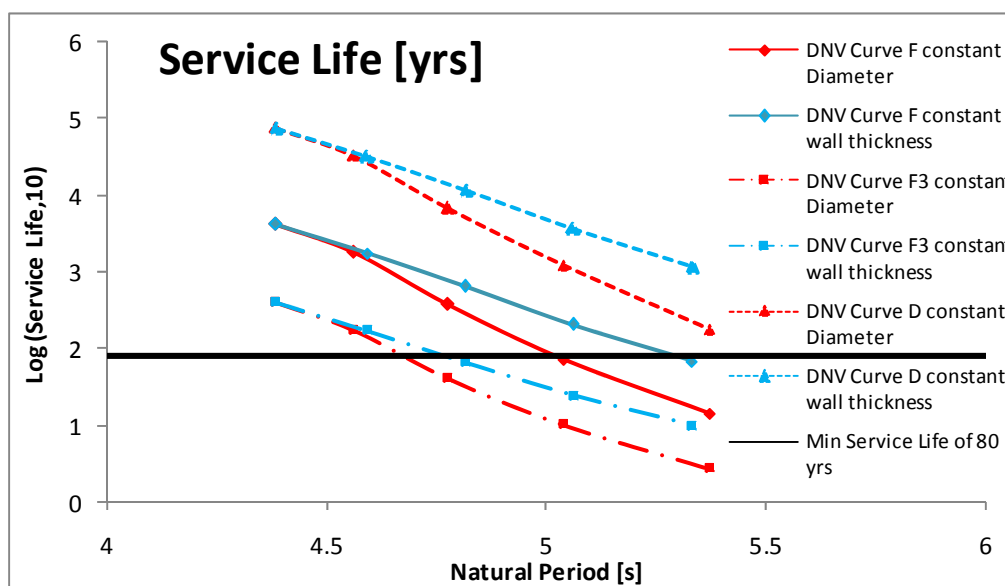
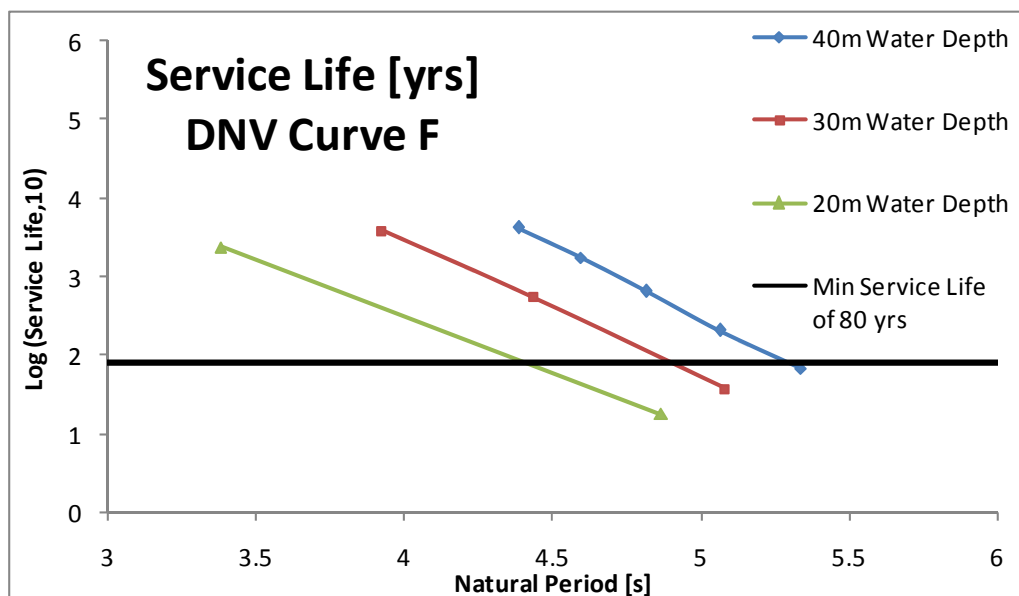


Figure 5-2 : Comparison Service Life Using Constant D and t_w at 40m Water Depth

Table 5-2 : Service Life of Monopile with Constant D of 400mm at 40m Water Depth

No	t_w	T_n	f_n	Service Life		
				DNV curve F	DNV curve F3	DNV curve D
	[cm]	[s]	[Hz]	[yrs]		
1	2.50	4.386	0.228	4201	400	76395
2	2.25	4.563	0.219	1806	175	32893
3	2.00	4.777	0.209	377	41	6819
4	1.75	5.040	0.198	74	10	1241
5	1.50	5.372	0.186	14	3	178

Figure 5-3 shows the MCT support structure service life at 40m, 30m and 20m water depth analyzed by DNV curve F. It is seen that the service life is also sensitive to water depth. The maximum recommended natural period to fulfil the required service life of 80 years are 5.3s, 4.9s and 4.4s for water depth of 40m, 30m and 20m respectively. The shallower depth requires stiffer structure or smaller natural period in order to fulfil the minimum service life of 80 years. Table 5-3 and Table 5-4 tabulate in detail the relationship between service life, natural period and monopile properties at 20m and 30m water depth.


Figure 5-3 : Comparison Service Life at Three Different Water Depth
Table 5-3 : Service Life of Monopile at 20m Water Depth

No	D	t_w	T_n	f_n	Service Life		
					DNV curve F	DNV curve F3	DNV curve D
	[cm]	[cm]	[s]	[Hz]	[yrs]		
1	25	2.5	3.382	0.296	2406	232	43960
2	25	2.0	3.658	0.273	634	63	11580
3	25	1.5	4.086	0.245	75	10	1287
4	20	2.5	4.867	0.205	18	3	242

Table 5-4 : Service Life of Monopile at 30m Water Depth

No	D	t _w	T _n	f _n	Service Life		
					DNV curve F	DNV curve F3	DNV curve D
	[cm]	[cm]	[s]	[Hz]	[yrs]		
1	32.5	2.5	3.924	0.255	3817	365	69377
2	32.5	2.0	4.265	0.234	553	57	10044
3	30	2.5	4.437	0.225	548	57	9960
4	27.5	2.5	5.080	0.197	38	6	598

5.3 Gravity Base Structure

The trend of service life of gravity base structure (GBS) has the similarity with monopile structure. However, the range of natural period of GBS is shifted to the left of the graph or shifted to a stiffer structure.

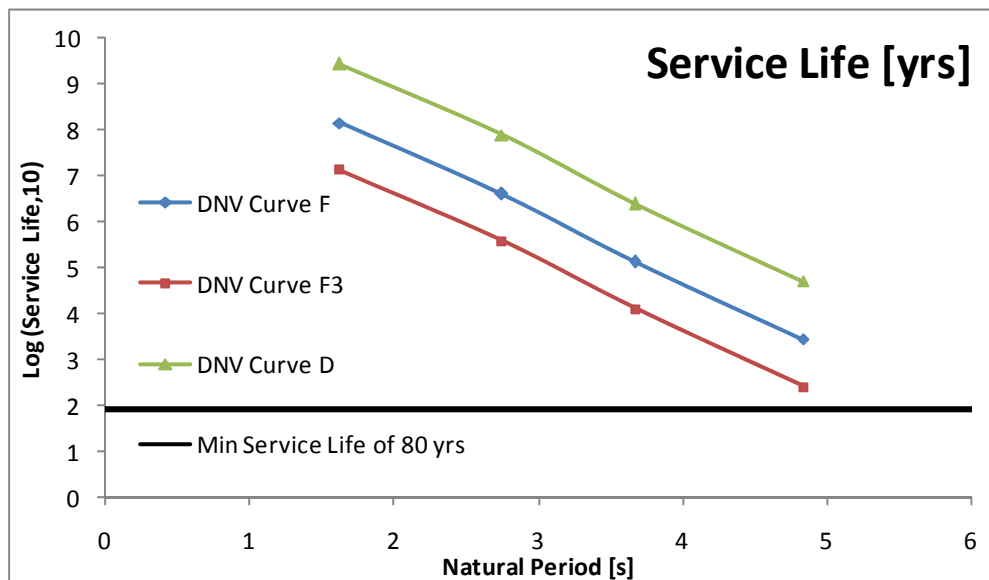


Figure 5-4 : Service Life of GBS at 40m Water Depth

Figure 5-4 shows the range of natural period (between 1.6s-4.8s) as function of GBS service life at 40m water depth. Similar to previous section, the DNV curve D has the highest service life followed by curve F and F3. Each curve has relatively linear relation between natural period and its service life (log function). As shown in the figure, all the connection details have the service life above the required service life of 80 years. Therefore, at this depth and particular natural period range, the most economical GBS support structure can be found at various alternatives. The most preferable would be at 4.8s of natural period which gives less properties and less mass required to survive from fatigue failure. Hereafter, Table 5-5 tabulates in detail the relationship between service life, natural period and GBS properties at 40m water depth.

Table 5-5 : Service Life of GBS at 40m Water Depth

No	D	t_w	T_n	f_n	Service Life		
					DNV curve F	DNV curve F3	DNV curve D
	[cm]	[cm]	[s]	[Hz]	[yrs]		
1	40	2.5	1.628	0.614	144520000	13443000	2692900000
2	30	2.0	2.752	0.363	4085249	380686	76952000
3	30	1.0	3.675	0.272	134041	12585	2484004
4	25	1.0	4.841	0.207	2771	263	50613

As the water depth reduces, the structure has to be stiffer to reach the required minimum service life of 80 years as shown in Figure 5-5 and Table 5-6. It can be seen that at natural period of 4.56s, the DNV curve F3 has service life less than required and down to 17 years of service life, on the other hand at water depth of 40m, the service life at 4.84s has 263 years. Thus, selection of natural period has to be made for fatigue design at this detail connection. However, for DNV curve F and D, both curves are still above the required service life time and can be used for design.

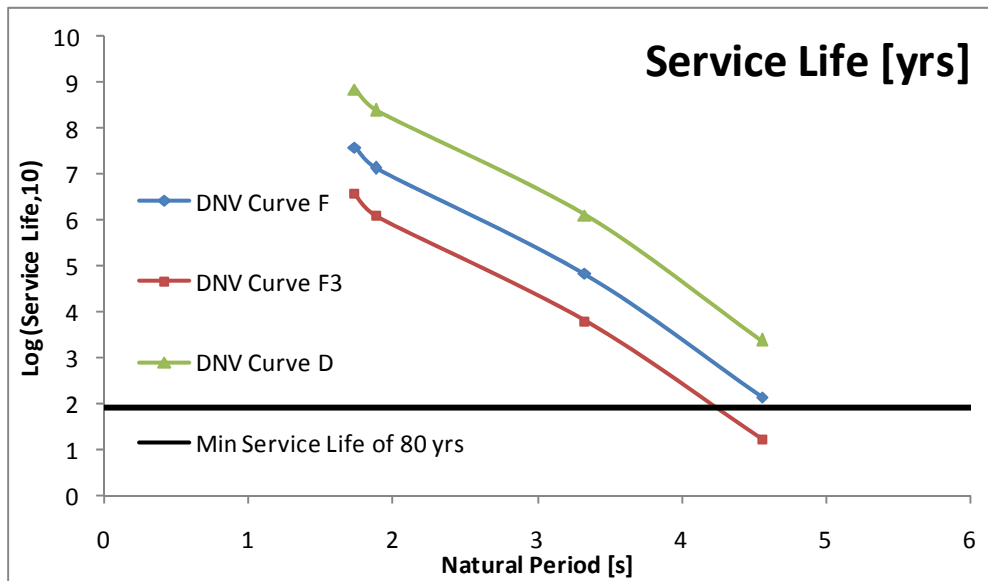


Figure 5-5 : Service Life of GBS at 30m Water Depth

Table 5-6 : Service Life of GBS at 30m Water Depth

No	D	t_w	T_n	f_n	Service Life		
					DNV curve F	DNV curve F3	DNV curve D
	[cm]	[cm]	[s]	[Hz]	[yrs]		
1	30	2.5	1.737	0.576	39178000	3644929	723090000
2	30	2	1.888	0.530	13334000	1240936	245240000
3	25	1	3.331	0.300	67742	6461	1255747
4	25	0.5	4.560	0.219	139	17	2447

Figure 5-6 and Table 5-7 show the detail connection service life as function of natural period at 20m water depth which has similar characteristic with previous discussion.

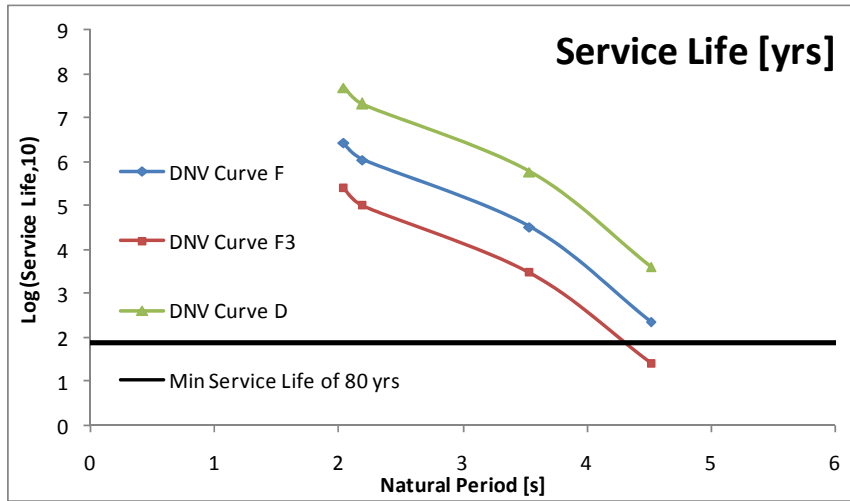


Figure 5-6 : Service Life of GBS at 20m Water Depth

Table 5-7 : Service Life of GBS at 20m Water Depth

No	D	t_w	T_n	f_n	Service Life		
					DNV curve F	DNV curve F3	DNV curve D
					[yrs]		
1	20	2.5	2.044	0.489	2651550	246906	48697000
2	20	2.0	2.197	0.455	1106505	103084	20399000
3	15	2.0	3.543	0.282	32792	3066	600452
4	15	1.0	4.516	0.221	235	27	4248

5.4 Tripod Structure

Tripod structure is a complex structure with a complex response. The response structure of tripod depends on site condition, structure arrangement and properties. This sophisticated structure has made tripod structure unpredictable, thus requires a unique design and very site specific. However, the proven design at reference location can be used as preliminary design at other location and modified as per actual environment condition.

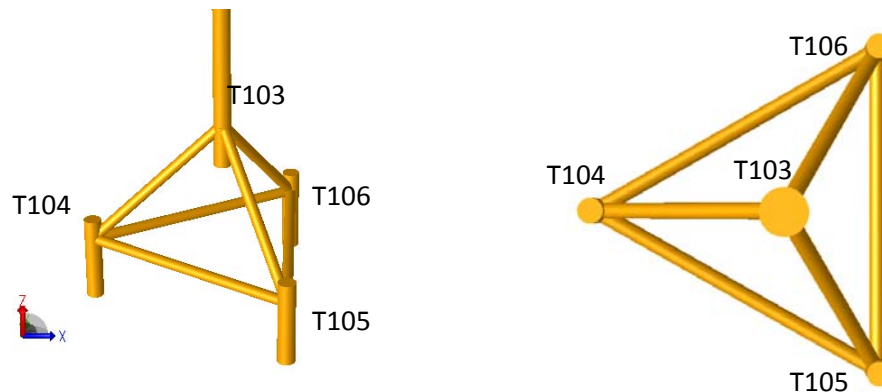


Figure 5-7 : Tripod structure 3D view and Top view

Figure 5-8 shows the service life of each joint of tripod structure at 40 m water depth. Joint T104, T105 and T106 have a similar geometry and properties thus the loadings are distributed evenly with relatively the same behaviour. On the other hand, joint T103 receives loadings from T104, T105 and T106 which makes this joint exposed three times more than others. As result, the service life of T103 joint is less than others.

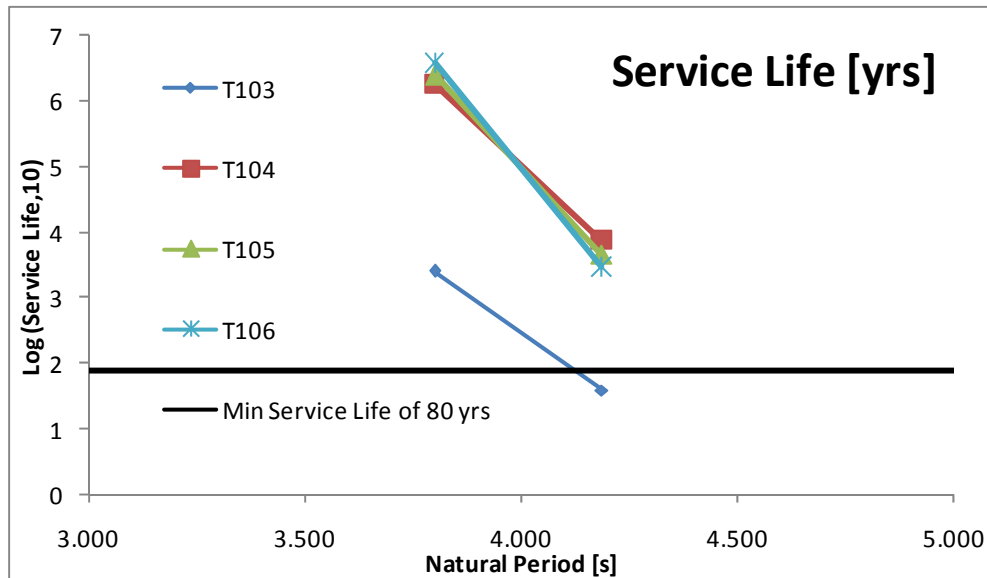


Figure 5-8 : Service Life of Tripod at 40m Water Depth

Table 5-8 tabulates the service life of tripod at 40m water depth at natural period ranging from 1.1s to 6.5s. As shown, the stiffer range up to 2.4s has infinite service life, meaning that the structure is safe from fatigue failure but over design. For upper range, 4.1s above, the service life is less than the required of 80 years, therefore, this range is failed due to fatigue. At natural period of 3.8s, the tripod has service life above the required thus this point is fatigue resistant with relatively efficient compare to other configurations. D and T_w represent diameter and wall thickness of pile while d and t_w are for diameter and wall thickness for pipe members T103-T104, T103-T105 and T103-T106.

Table 5-8 : Service Life of Tripod at 40m Water Depth

No	D	T_w	d	t_w	T_n	f_n	Service Life (API-AXP)			
							T103	T104	T105	T106
							[yrs]			
1	40	2.5	25	1.5	1.173	0.852	INFINITE	INFINITE	INFINITE	INFINITE
2	25	1.5	20	1.0	2.419	0.413	INFINITE	INFINITE	INFINITE	INFINITE
3	25	0.8	16	0.5	3.801	0.263	2568	1818264	2477354	3755557
4	25	0.5	16	0.5	4.186	0.239	40	7603	4678	2945
5	20	1.0	10	0.5	6.534	0.153	14	301	365	1424

6 ECONOMICS AND OPTIMIZATION

6.1 Introduction

This chapter covers the possible economics and optimization that can be applied in the fatigue analysis of marine current turbine element. Two main concerns of total costs are coming from capital or initial or construction cost and cost during operating condition including maintenance of MCT.

The overall financial analysis in MCT design starting from capital cost to maintenance and operating cost are explained in section 6.2 followed by support structure selection at section 6.3 Optimization in fatigue design based on cathodic protection, weld improvement and inspection strategy will be discussed in section 6.4, 6.5 and 6.6 respectively.

6.2 Financial Analysis

The economic aspect of energy development and exploration is basically comprised into four main subjects which are capital cost, operation and maintenance (O&M) cost, fuel cost and external cost. The economic aspect of renewable energy such as wind energy and hydro energy is affected by capital and O&M costs. Since this technology is relatively new, the capital cost for renewable energy is considered high. But, in the future, the cost is likely to decrease as new technology developed, new markets opens up, and the total installed capacity increases.

The main idea of MCT energy converter was to find a low cost alternative energy resource. A successful financial analysis is defined by financial indicators, such as Net Present Value (NPV), Internal Rate of Return (IRR), Payback Period and Value Investment Ratio (VIR). The IRR is most commonly used to measure the benefits of any financial system. For example, investment in fund has 5%, utility has 6%, oil and gas has 8% and wind energy (with: 2000 \$/KW; load factor 35 % and power price 0.047 \$/kWh) has 2.3% of IRR (source: SHELL, 2010).

High value of IRR is more attractive to the stakeholders. Based on SHELL research on Offshore Wind Turbine (OWT), the enhancement of IRR could be reached by decreasing construction costs, increasing power price, increasing capacity factor and decreasing maintenance costs as described in Figure 6-1.

At present, due to lack of data and none of the MCT's are installed in field yet therefore detail financial analysis of MCT cannot be estimated.



Figure 6-1 : IRR Sensitivity of Offshore Wind Farm (Shell, 2010)

6.3 Support Structure Selection

The analysis result from previous chapter shows that each MCT support structure has their own advantage and limitation. Discussion on advantages and limitations are outlined in this section.

6.3.1 Monopile Structure

Monopile type structures are appropriate for calm environment of shallow or intermediate water level (up to 30m depth) with soft soil characteristics such as clay and sand. The single pile with slender configuration makes monopile structures have relatively large natural period to keep it economically profitable. This excessive natural period is prone to dynamic responses and resonance. For Bali strait, per year chance of resonance is up to 9% if the natural period is set at 4.5 second (see Figure 4-6). However, the effect of resonance can be reduced by the hydrodynamic damping of the rotating turbine [38]. On the other hand, monopile structures can be installed in soft soil characteristics by conventional pile driving and boring technique. Another note for monopile structures are the effect of excessive deflection at the top of structure and should be safe in service limit state (SLS) point of view.

6.3.2 Gravity Base Structure

Gravity base structures are appropriate for intermediate (20m to 80m) water depth with hard or rocky soil characteristics. The hardness of soil characteristics makes it impossible and not economical to bore or drive, thus the foundation of GBS is held in place by gravity and

often built in with tanks or cells which can be used to control the buoyancy of the finished GBS. Soil or foundation preparation is also required at relatively large area before placing GBS into its position.

For Bali strait which is covered by hard coral reef, GBS is suitable to be used. This stiff structure has bigger strength resistance and has relatively small deflection at the top of structure. In addition, GBS offers less material cost compare to monopile and tripod type structures. However, the coral reef area that is converted into GBS foundation has to be analyzed carefully in accordance with Environment Impact Assessment.

6.3.3 Tripod Structure

Tripod structures are appropriate for intermediate (20m to 80m) water depth with soft soil characteristics. This structure is the extension of monopile structure with additional three legs to accommodate stiffness and strength of the structure. In practice, tripod structures have the strength of GBS in form of monopile structure.

For Bali strait which has soft soil at seabed combined with rocky soil at certain depth below; tripod structures offer an economical option. The combination of soil friction and bearing tip leads into a rigid foundation. Thus, the structure becomes stiffer and less affected by fatigue failure. However, installation procedure has to be considered carefully since it requires pile driving or boring in the vicinity of coral reef including EIA assessment.

6.4 Cathodic Protection

Steel structures submerged in water are susceptible to corrosion. The fatigue design of steel structures submerged in water is assumed to be adequately protected by a cathodic protection system. Four methods of cathodic protection can be applied in order to fulfil the requirements, which are:

- Corrosion allowance, adding extra reserve wall thickness to compensate steel consumption.
- Protective coating, special painting to prevent corrosion, applied in vicinity of dynamically changing environment such as in the water surface area.
- Impressed current, active electrical current to prevent electrochemical process of corrosion at submerged steel.
- Anodes, sacrificial material creating electrochemical process to prevent corrosion at submerged steel.

In oil and gas industry, anodes and protective coating are the most commonly used cathodic protection system for continuously submerged steel material and area at water surface elevation respectively. Numbers or anodes should be calculated accordingly due to the

needs of protection. Otherwise, overprotection by using excessive anodes can cause hydrogen production which can lead to embrittlement and significantly reduce the fatigue lives. Minimal production of hydrogen can be expected by using conventional aluminium and zinc anodes for normal steel structures. If, for instance, magnesium anode or higher strength steel (yield stress over 400 MPa) is used, the threat from hydrogen embrittlement might occur and therefore it should be examined.

6.5 Weld Improvement

Improvement in fatigue life is achieved by grinding weld technique. However this technique should not be used during design phase because grinding is more expensive compare to conventional welding. Redesign should be conducted if inadequate fatigue lives occur at design phase. On the other hand, if fatigue problem occurs during construction or operating condition and redesign option is not feasible, weld grinding may be used.

To be noted that ground weld improves the fatigue life due to increment of the initiation time of a defect without improvement of propagation time and therefore the early warning of crack development is less pronounced.

6.6 Inspection Strategy

Analytical prediction for structure fatigue performance provides valuable input for inspection strategy, especially for submerged structures. The strategy is not only based on fatigue criteria but also other things such as weather and current speed. However, for new structure design, a comfortable margin in calculation design fatigue lives provides a cost effective investment compared to marginal design which requires more extensive fatigue inspection.

For existing structures with low analytical fatigue lives, the inspection interval may be updated based on a good in-service fatigue performance. An assessment of fatigue crack growth behaviour for welded connection shows that the time for a defect to grow to a size that reliably detected by practical underwater inspection technique is less than half of the time for through thickness crack development. This means that an early warning of crack growth is introduced as the remaining life is at least equal to the initiation period up to time of detectable size. If defect free is shown by a connection after given service period, the remaining life will normally be at least equal to the service life to date. And if the updated service life is significantly over the analytical fatigue life, it means that the analysis has more conservative value and therefore the inspection interval may be increased accordingly.

7 CONCLUSION AND RECOMMENDATION

7.1 Conclusion

After conducting this study, the main conclusions drawn are summarised in the following:

1. Indonesia has many potential tidal energy resources. However, in this thesis, reference site between Java and Bali islands is selected in order to support tourism in Bali Island which requires more energy supply.
2. At the reference site, the frequency-based methodology with two independent approach of fatigue loading (wave and current induce turbine) is able to simulate the fatigue damage calculation.
3. The simulation of fatigue damage comprises three different support structures (monopile, gravity based and tripod) at three different water depth (20, 30 and 40 meters). Those simulations are selected in regards to find out the most effective support structure based on production cost, construction and maintenance.
4. The lower wave height and shorter wave period derives the inertia component of wave loading more important in fatigue analysis compare to extreme storm analysis. Therefore, selection of inertia coefficients and equivalent volumes for members and in particular for complex assemblies requires careful attention.
5. The fatigue damage analysis shows that DNV curve D has the longest service life compare to curve F followed by curve F3. This curve selection is based on connection details design at the MCT support structure.
6. At the same structure natural period, properties with smaller cross section area and inertia have less service life. The cross section area and inertia of particular connection represent the welding area, therefore, less cross section properties derive less fatigue strength.
7. The service life is also sensitive to water depth. The shallower water depth requires stiffer structure or smaller natural period in order to fulfil the minimum service life of 80 years.
8. The study of fatigue design on MCT support structure in Bali Strait shows that the fatigue life design has many property alternatives in order to fulfil required service life of 80 years (20 years design life with factor of safety 4.0). For example, from 400mm pile diameter x 20mm wall thickness of monopile structure using DNV curve F connection detail at 40m water depth to 250mm pile diameter x 10mm wall thickness of gravity base structure (GBS) using DNV curve F3 connection detail at 40m water depth.

9. Contrary to the offshore wind turbine with natural period at soft-soft range, the recommended natural period range for MCT is placed at soft-stiff range. This because of the MCT support structure requires stiffer and more compact structure as they are exposed to a more severe loading compare to OWT. The operating turbine exposed to wave and current are the main cause of this difference. It provides larger catching area hence a larger wave and current loading occur at this stage.
10. Each type of MCT support structure has its own benefits. Based on experiences in the oil and gas exploration industry, monopile support structure is appropriate for shallow water with soft soil characteristic (clay and sand). GBS support structure is suitable for intermediate water depth at rocky or hard soil characteristic. And tripod support structure is recommended for intermediate water depth at soft soil characteristic (clay and sand). For Bali strait, GBS and tripod structure are suitable in regards of site soil characteristics (hard soil and combination of soft-hard soil).
11. The methodology has been tested for three different type of support structure. It shows that this methodology can be used as general guidance for fatigue design of MCT support structure.
12. Although the fatigue design for Bali strait has service life above the required life time, however for detailed design, a complete and comprehensive environment data (wave, current and soil) is required to conduct a proper fatigue design assessment.
13. Fatigue design is a unique design for a particular location at particular environment data (wave, current and soil). Therefore, It is only valid for particular location and cannot be generalized.

7.2 Recommendation

The study of fatigue design on MCT support structure has enhanced the understanding of fatigue damage assessment including its service life, especially at Bali strait. This study might be the first study of fatigue assessment in MCT support structure and should be considered an opening to a further renewable energy development. Recommendations for further research therefore formulated here after.

Environment Data and Modelling

The environment modelling as representation of actual condition in reference site location is very critical and has to be as accurate as possible. Unlike the oil and gas exploration platform which requires one compact platform, tidal energy extraction requires large area for marine

current turbine farm. Therefore, efficiency at each MCT will reduce production cost significantly. The environment data comprises wave, current and soil characteristics.

The wave data for oil and gas industry can be used in MCT development because the sea is well presented by the long-term seastate. On the other hand, current data should be improved and be analyzed more accurately as per wind data for offshore wind turbine development. The current velocity data should be analyzed as per actual condition in the field at each elevation of interest. The soil data should represent the spring characteristics of the soil in order to model pile-soil interaction. This pile-soil interaction has been used in the oil and gas industry as the most effective linearization modelling of foundation and therefore it's applicable for MCT development.

Computer Model

Computer model is as important as environment data. Precise environment data collaborates with accurate computer modelling derives effective and efficient design which leads to economical result. The Structure Analysis Computer System (SACS) is able to translate actual condition into compute model with relatively reliable accuracy. However, there are some limitations in SACS such as: (1) the fatigue calculation is assumed to be independent at each other due to SACS module availability, (2) the user has to be familiar with SACS, (3) low frequency cut off in order to avoid excessive loading from constant wave steepness approach, (4) the analysis procedural has to be followed and iterated in order to get the accurate result, (5) This software is designed for offshore platform therefore adjusted modelling is conducted.

Presently, there is no particular software dedicated for marine current turbine fatigue design. Therefore, other similar computer program can be used to assess and simulate fatigue damage of MCT. Comparing SACS to commercial software is also useful to check the result and study if there is an anomaly or differences. Recommended softwares are STAAD Pro, SESAM and softwares for offshore wind turbine.

Fatigue Damage Assessment

Based on offshore wind turbine technology, the fatigue damage analysis and calculation has many varieties. Combination between time series and frequency based calculation are the main method for fatigue damage calculation. The varieties of calculation appear in the market are because of company preference, software development and the users. For detail

design it is recommended to use time series approach or frequency based to extract the actual condition for both wave and current loadings. For screening phase, frequency based is preferred due to time efficiency.

Environment Impact Assessment (EIA) in Bali Strait

Bali is well known as island of god, rich with species especially underwater biota. This beauty attracts local tourist as well as international tourist and becomes Indonesia's top destination with tremendous revenue per year. As we try to put a new technology in Bali water and every new technology requires environment impact assessment. Therefore EIA for projects, construction, transportation, installation, operation and maintenance should be assessed. For MCT projects, the effect of tidal energy extraction could give negative effect to the environment and unfortunately, at present, this type of impact is rarely investigated especially in South East Asia region. Hence, EIA study in Bali strait should be conducted at the very first time.

Indonesia

One of Indonesia's major problems is lack of reliable long-term data. There are more sites that are applicable for MCT development but many of those have no data or not reliable to be used. Lack of site measurement is the main problem. However, this problem could be solved with intensive site measurement starting with potential site such as Capalulu Strait, Berau Bay and Malacca Strait.

REFERENCES

- [1] Ainsworth, D. & Thake, J., 2006. Final report on preliminary works associated with 1 MW tidal turbine. DTI Technology Programme: New and Renewable Energy.
- [2] Bahaj, A. & Myers, L., 2003. Fundamentals Applicable to the Utilisation of Marine Current Turbines for Energy Production. *Renewable Energy*, 28, pp.2205-11.
- [3] Bahaj, A. & Myers, L., 2004. Analytical Estimates of Energy Yield Potential from the Alderney Race (Channel Islands) using Marine Current Energy Converters. *Renewable Energy*, 29, pp.1931-45.
- [4] Barltrop, N.D.P. & Adams, A.J., 1991. *Dynamics of Fixed Marine Structures*, Butterworth-Heinemann Ltd, Oxford, (1991). ISBN 0-7506-1046-8.
- [5] Batten, W., Bahaj, A., Molland, A. & Chaplin, J., 2006. Hydrodynamics of Marine Current Turbines. *Renewable Energy*, 31, pp.249-56.
- [6] Black & Veatch, 2005. Phase II UK Tidal Stream Energy Resource Assessment. London: The Carbon Trust.
- [7] Black & Veatch, 2005. Tidal Stream Energy Resource and Technology Summary Report. Middlesex: The Carbon Trust.
- [8] Blunden, L. & Bahaj, A., 2006. Initial Evolution of Tidal Stream Energy Resources at Portland Bill, UK. *Renewable Energy*, 31, pp.121-32.
- [9] Blunden, L. & Bahaj, A., 2007. Tidal Energy Resource Assessment for Tidal Stream Generators. In IMechE Vol.221 Part A: Power and Energy.
- [10] Burton, T., Sharpe, D., Jenkins, N. & Bossangi, E., 2001. *Wind Energy Handbook*. New York: Wiley.
- [11] Charlier, R.H., 1982. *Tidal Energy*. New York: Van Nostrand Reinhold Company Inc.
- [12] Corten, G.P., 2001. *Flow Separation on Wind Turbine Blades*, PhD Thesis, Utrecht University. ISBN 90-393-2582-0.
- [13] da Rosa, A.V., 2005. *Fundamentals of Renewable Energy Processes*. London: Elsevier Academic Press.
- [14] Energy Systems Research Unit's of The University of Strathclyde in Glasgow, 2006. Marine Current Resource and Technology Methodology. [Online] Available at: http://www.esru.strath.ac.uk/EandE/Web_sites/05-06/marine_renewables/home/welcome.htm. On 1 June 2011.
- [15] Environmental Change Institute, 2005. Characteristics of the United Kingdom Tidal Current Power Resource. The Carbon Trust.
- [16] EU Commission, 1996. The exploitation of tidal marine currents.

- [17]Fraenkel, P., 1999. Tidal currents: a major new source of energy for the millennium. London: ICG Publishing Ltd.
- [18]Fraenkel, P., 2007. Marine current turbines: pioneering the development of marine kinetic energy converters. In IMechE Vol. 221 Part A: J. Power and Energy., 2007.
- [19]Freris, L. & Infield, D., 2008. Renewable Energy in Power Systems. Chichester, West Sussex: John Wiley & Sons Ltd.
- [20]Garrett, C. & Cummins, P., 2005. Generating Power from Tidal Currents in Channels. In R. Soc. Land A.
- [21]Hermawan & Hadi, S.P., 2006. Existing Sustainable (Renewable) Energy System in Indonesia. In The 2nd Joint International Conference on Sustainable Energy and Environment. Bangkok, 2006.
- [22]Hydro-Oceanographic Service Indonesian Navy, 2009. Tide Tables of Indonesian Archipelago. Jakarta: Hydro-Oceanographic Service Indonesian Navy.
- [23]Hydro-Oceanographic Service Indonesian Navy, 2009. Tide Tables of Indonesian Archipelago. Jakarta: Hydro-Oceanographic Service Indonesian Navy.
- [24]Indonesia's Centre for Data and Information on Energy and Mineral Resources , 2008. Indonesia Energy Statistics 2008. Jakarta: Ministry of Energy and Mineral Resources.
- [25]Indonesia's Centre for Data and Information on Energy and Mineral Resources, 2006. Blueprint of Indonesia's Energy Management 2006 - 2010. Jakarta: Ministry of Energy and Mineral Resources.
- [26]Indonesia's Centre for Data and Information on Energy and Mineral Resources, 2008. Key indicator of Indonesia energy and mineral resources. Jakarta: The Ministry of Energy and Mineral Resources.
- [27]Kaltschmitt, M., Streicher, W. & Wiese, A., 2007. Renewable Energy: Technology, Economics, and Environment. New York: Springer.
- [28]Kühn, M., 2001. Dynamics and Design Optimisation of Offshore Wind Energy Conversion Systems Institute for Wind Energy, Delft University of Technology. ISBN 90-76468-07-9.
- [29]LAPI ITB, 2005. Final report of Metocean Design Criteria for General Kangean Block Area, 29 August 2005.
- [30]Maunsell, F. & Metro, P., 2007. Scottish Marine Renewable Strategic Environmental Assessment (SEA): Environmental Assessment. EIA Report. The Scottish Executive.
- [31]Millar, D.L., 2007. Wave and Tidal Power. In F. Armstrong & K. Blundell, eds. Energy. Beyond Oil. Oxford: Oxford University Press, pp.50-70.

- [32]Myers, L.E., 2006. Operational Parameters of Horizontal Axis Marine Current Turbines. PhD Thesis. Southampton: University of Southampton.
- [33]Myers, L. & Bahaj, A., 2005. Simulated Electrical Power Potential Harnessed by Marine Current Turbine Arrays in the Alderney Race. *Renewable Energy*, 30, pp.1713-31.
- [34]Pandey, V.K. & Pandey, A.C., 2007. Turbulent Kinetic Energy and Its Dissipation Rate of the Indonesian Throughflow Region via Lombok and Savu Straits. *Journal of India Geophysic Union*, 11(2), pp.117-22.
- [35]Pangastuti, W., 2005. Study of tidal use in Seribu Islands Area. Bsc Final Project. Bandung: Bandung Institute of Technology.
- [36]Petroleum and natural gas industries, ISO 19901-1, 2005. Specific requirements for offshore structures Part 1: Metocean design and operating considerations International Organization for Standardization, Geneva, Switzerland.
- [37]Tempel, J. van der & Molenaar, D.P., 2002. Wind Turbine Structural Dynamics: a Review of the Principles for Modern Power Generation, Onshore and Offshore, Publication, *Wind Engineering*, Volume 26, No. 4.
- [38]Tempel, J. van der, 2006. Design of Support Structures for Offshore Wind Turbines, PhD Thesis, Delft University of Technology.
- [39]Vugts, J.H., 2000. Considerations on the dynamics of support structures for an OWEC Section Offshore Technology, Delft University of Technology
- [40]Vugts, J.H., 2001. Handbook of Bottom Founded Offshore Structures, Lecture notes, Delft University of Technology.
- [41]Weisstein, E.W., 2011. Fast Fourier Transform.
<http://mathworld.wolfram.com/FastFourierTransform.html>. On 16 May 2011.
- [42]Wilson, E.L., 2002. Three-Dimensional Static and Dynamic Analysis of Structures: A Physical Approach with Emphasis on Earthquake Engineering, 3rd Ed.

APPENDICES

Appendix A1 Environment Data

Appendix A2 Computer Model Plot

Appendix A3 Output Listing